Metamodel-based pattern recognition approach for real-time identification of earthquake-induced damage in historic masonry structures

Enrique García-Macías[a,*], Ilaria Venanzi[a], Filippo Ubertini[a]

[a]*Department of Civil and Environmental Engineering, University of Perugia. Via G. Duranti, 93 - 06125 Perugia, Italy.*

Abstract

Damage localization/quantification through vibration-based Structural Health Monitoring (SHM) is commonly performed by inverse calibration of a numerical model. Nevertheless, the numerous simulations required in the associated optimization problem pose a daunting obstacle when applied to real-time SHM. Particularly critical are heritage buildings, whose complex geometries often require computationally intensive modellings. In this light, this paper presents a novel earthquake-induced damage identification approach for historic masonry structures. This relies upon the use of a computationally efficient meta-model suited for real-time system identification. The optimization problem is formulated accounting for discrepancies between numerical and experimental resonant frequencies and mode shapes. Damage localization/quantification is enabled by multivariate analyses of continuously identified model parameters. A real medieval tower is presented as a case study, and several damage scenarios are simulated and used for validation. The reported results pave the way for the development of next-generation long-term vibration-based SHM systems with real-time damage identification capabilities.

Keywords: Damage localization, Historic buildings, Meta-model, Model updating, Operational Modal Analysis, Structural health monitoring, Surrogate models.

1. Introduction

There is a broad consensus today on the importance of adopting SHM strategies for preventing catastrophic failures and excessive infrastructure downtimes [1–3]. In particular, tragic collapses of civil structures such as the Genoa bridge in August 2018, or the loss of invaluable heritage structures such as the civic tower of Pavia in 1989 have evidenced the large risks associated with ageing degradation and inefficient maintenance [4, 5]. This has promoted a large volume of research on SHM since 1970s, although the reality is that these research efforts have yielded relatively few routine industrial applications [1]. Amongst the reasons explaining this slow technological transfer [3], it is worth stressing the lack of performance validation of damage identification techniques on full-scale structures under real operating conditions.

Among the wide variety of SHM technologies present in the literature, dynamic testing has attracted most of the attention due to its global damage assessment capabilities and minimum intrusiveness. These techniques utilize modal parameters (i.e. resonant frequencies, mode shapes and damping ratios) as damage-sensitive features since these depend upon the mass, stiffness, and energy dissipation properties of structures [6–12]. Modal properties are highly affected by environmental conditions, thereby such techniques are mainly effective when implemented in a long-term monitoring program. This allows the definition of a healthy/baseline dataset, often referred to as the training period, alongside the creation of statistical models for the subtraction of environmental effects [13–18]. In this manner, the appearance of damage can be detected by multivariate statistical analysis of anomalies in the time series of modal properties. In this light, a variety of successful applications to diverse structural typologies can be found in the literature (see e.g. [19–21]), which has favoured vibration-based damage detection to become a quite consolidated and mature approach. Unfortunately, their application for damage localization and quantification has not been so successful [3]. This usually requires the use of numerical models linking damage mechanisms and the intrinsic mass/stiffness/damping properties of structures to their modal signatures [22, 23]. Hence, the effectiveness of this approach largely depends upon the accuracy of the model and the way material constitutive properties and damage mechanisms are modelled. In this regard, Structural Identification (St-Id) or model updating aims to bridge the gap between models and real systems by tuning the model parameters in such a

*Corresponding author. Department of Civil and Environmental Engineering, University of Perugia. Via G. Duranti, 93 - 06125 Perugia, Italy. phone: +39 075 585 3908; fax: +39 075 585 3897

Email addresses: `enrique.garciamacias@unipg.it` (Enrique García-Macías), `ilaria.venanzi@unipg.it` (Ilaria Venanzi), `filippo.ubertini@unipg.it` (Filippo Ubertini)

way that the mismatch between experimental and theoretical observations/data is minimized. Nevertheless, despite the obvious motivation of St-Id, potential public and private end-users remain sceptical about its usefulness for the maintenance and management of civil infrastructure [3]. This is chiefly due to the lack of compelling evidences of its effectiveness in the literature, where too simple models and prescriptive codes are generally used [24].

One of the main obstacles for the extensive implementation of St-Id in engineering practice stems from the difficulties involved in the use of computationally intensive numerical models into automated long-term SHM systems. In this context, cultural heritage (CH) structures constitute a remarkable example since these usually feature complex geometries requiring fine discretizations. Typically, damage identification is achieved by the inverse calibration of a finite element model (FEM) through a non-linear optimization problem. Such an optimization usually requires an elevated number of model evaluations, resulting in large computational times that are incompatible with real-time SHM systems. Hence, most research works in the literature have limited to the use of simplified numerical models or discrete St-Id. Nonetheless, recent advances in the use of surrogate models have opened a new horizon for real-time St-Id-enabled damage identification [25–29]. A noteworthy contribution was made in this regard by Cabboi et al. [22] who reported the damage identification of a stone-masonry tower using continuous Operational Modal Analysis (OMA) and a surrogate Response Surface Model (RSM). The St-Id was achieved using an objective function accounting for differences between experimental resonant frequencies and the theoretical predictions of the surrogate model. The effectiveness of the proposed approach was evaluated through simulated damage scenarios obtained by decreasing the elastic moduli of certain parts of the model. In this line, recent contributions by the authors [28, 29] presented an enhanced version of the methodology by Cabboi et al., where the St-Id was performed with a functional comprising not only resonant frequencies but also mode shapes. The presented results demonstrated the ability of the proposed approach to identify the environmental effects upon the intrinsic elastic properties of a masonry tower. Despite the encouraging results, several issues still need to be addressed to broaden its application to damage identification and assert its reliability. These include: i) appraisal of the effectiveness of surrogate model-based St-Id when dealing with full-scale structures and realistic damage scenarios; ii) assessment of the importance of accounting for the time evolution of mode shapes; iii) adoption of pattern recognition techniques to remove environmental effects and so enable early-damage identification; iv) design and evaluation of proper regularization approaches to minimize ill-conditioning limitations in the St-Id; v) implementation of novelty detection approaches to automate the damage identification process.

As a solution to the afore-mentioned shortcomings, the present work proposes an enhanced version of the surrogate model-based damage identification approach in [28, 29]. Unlike previous approaches, the newly proposed method incorporates statistical pattern recognition and anomaly detection techniques. Such an upgrade is crucial for early damage identification because, as previously reported by the authors [29], environmental factors considerably affect the model fitting parameters and may mask the appearance of damage. Specifically, the effectiveness of three different statistical models for filtering out these effects is explored, including Multiple Linear Regression (MLR), Principal Component Analysis (PCA), and Autoassociative Neural Networks (ANNs). Afterwards, automated damage detection is enabled by novelty analysis of the residuals between the identified model parameters and the predictions of a statistical model constructed over a baseline/training period. The effectiveness of the proposed methodology is ascertained with a case study of a 41 m high civic historic tower located in the city of Perugia in Italy, named *Torre degli Sciri*. The tower has been continuously monitored during three weeks with an environmental/dynamic SHM system. The modal features of the tower have been extracted by automated OMA and used in the inverse calibration of a 3D FEM of the structure. The model updating accounts for the time evolution of both resonant frequencies and mode shapes, and a new regularization approach for tackling differential parameter sensitivities and minimizing ill-conditioning limitations is developed. Computational times are made compatible with real-time SHM by using an inexpensive RSM, which replaces the original FEM. Finally, the present approach is validated for simulated earthquake-induced damage scenarios with increasing severity degrees. To do so, a pushover analysis of the 3D FEM of the Sciri Tower is conducted, and a non-linear modal analysis of the FEM allows to include the simulated scenarios in the time series of experimental resonant frequencies and mode shapes. The presented results and discussion highlight the importance of including the experimental mode shapes in the St-Id for alleviating ill-conditioning in the solution, as well as the need for controlling their modal complexity.

The remainder of this paper is organized as follows. Section 2 outlines the proposed surrogate model-based ST-Id for automated damage identification. Section 3 describes the investigated case study of the Sciri Tower, the continuous dynamic/environmental SHM system, the development of a 3D FEM of the structure, and the initial calibration of the model using a GA. Section 4 reports the results of the non-linear incremental analysis carried out in order to generate synthetic earthquake-induced damage scenarios for validation purposes. Section 5 presents the results and discussion of the application of the proposed methodology to the investigated case study. Finally, Section 6 concludes the paper.

2. Damage identification enabled by automated surrogate model-based St-Id

The present surrogate model-based damage identification methodology represents an enhanced version of the previously published approach by the authors in reference [29]. The newly proposed approach is sketched in Fig. 1 and comprises the following three consecutive steps:

(A): **Initial calibration of the FEM**: The initial FEM is constructed based on available structural drawings, on-site inspections, and surveys of the material properties. Additionally, a series of assumptions must be usually made to complete the definition of the model. These may concern several aspects such as boundary conditions, material homogeneity or structural connectivity. Therefore, the initial FEM may involve considerable sources of uncertainty that should be minimised before constructing the subsequent surrogate model. To do so, certain parameters of the FEM (typically mass density and elastic moduli of certain structural members) are tuned with the aim of minimizing the differences between the numerical modal features and those identified experimentally from an initial ambient vibration test (AVT). In this work, this is conducted using a GA as reported hereafter.

(B): **Construction of the surrogate model**: Based upon the previously tuned FEM, a surrogate model is constructed in order to set up an analytical relationship between certain damage-sensitive model parameters and the modal features of the structure. This black-box representation of the FEM offers a computationally efficient solution to perform iterative model updating procedures.

(C): **Automated surrogate model-based St-Id and anomaly detection**: This last step regards the automated OMA of the structure, fitting of the damage-sensitive model parameters, and identification of damage in the shape of statistical anomalies in the time series of the fitting parameters. By virtue of the limited computational demand of the surrogate model, this procedure can be readily implemented in the framework of a real-time SHM system and provide online damage identification capabilities.

(C.1) <u>Automated OMA</u>: The modal features of the structure are experimentally identified by automated OMA of periodically recorded ambient vibrations. The outcome of this stage at every step j comprises a set of resonant frequencies f_j and mode shapes φ_j.

(C.2) <u>Surrogate-based model updating</u>: The design variables at step j, $\overline{\mathbf{x}}_j$, are fitted to minimize the mismatch between the last set of experimental modal features and the estimates of the surrogate model.

(C.3) <u>Model parameters tracking</u>: The design variables fitted in the preceding step $\overline{\mathbf{x}}_j$ are stored in the j-th row of a matrix $\overline{\mathbf{X}}$. This matrix contains the time series of the fitted model parameters by columns.

(C.4) <u>Pattern recognition</u>: From an initial baseline dataset where the structure is assumed to remain in healthy condition, a statistical model is constructed in order to phase out the fluctuations in the time series of fitted model parameters induced by environmental/operational effects in normal operating conditions.

(C.5) <u>Anomaly detection</u>: The initiation of a damage mechanism can be identified through novelty analysis of the residuals between the fitting parameters and the estimates of the previously built statistical model. Upon setting a statistical threshold associated with a certain confidence level, it is possible to trigger an alarm system when anomalies are detected in the shape of residuals consistently overpassing the threshold. Since every design variable relates to the intrinsic stiffness of a specific element/region of the structure, anomalies in their time series directly indicate the location of damage.

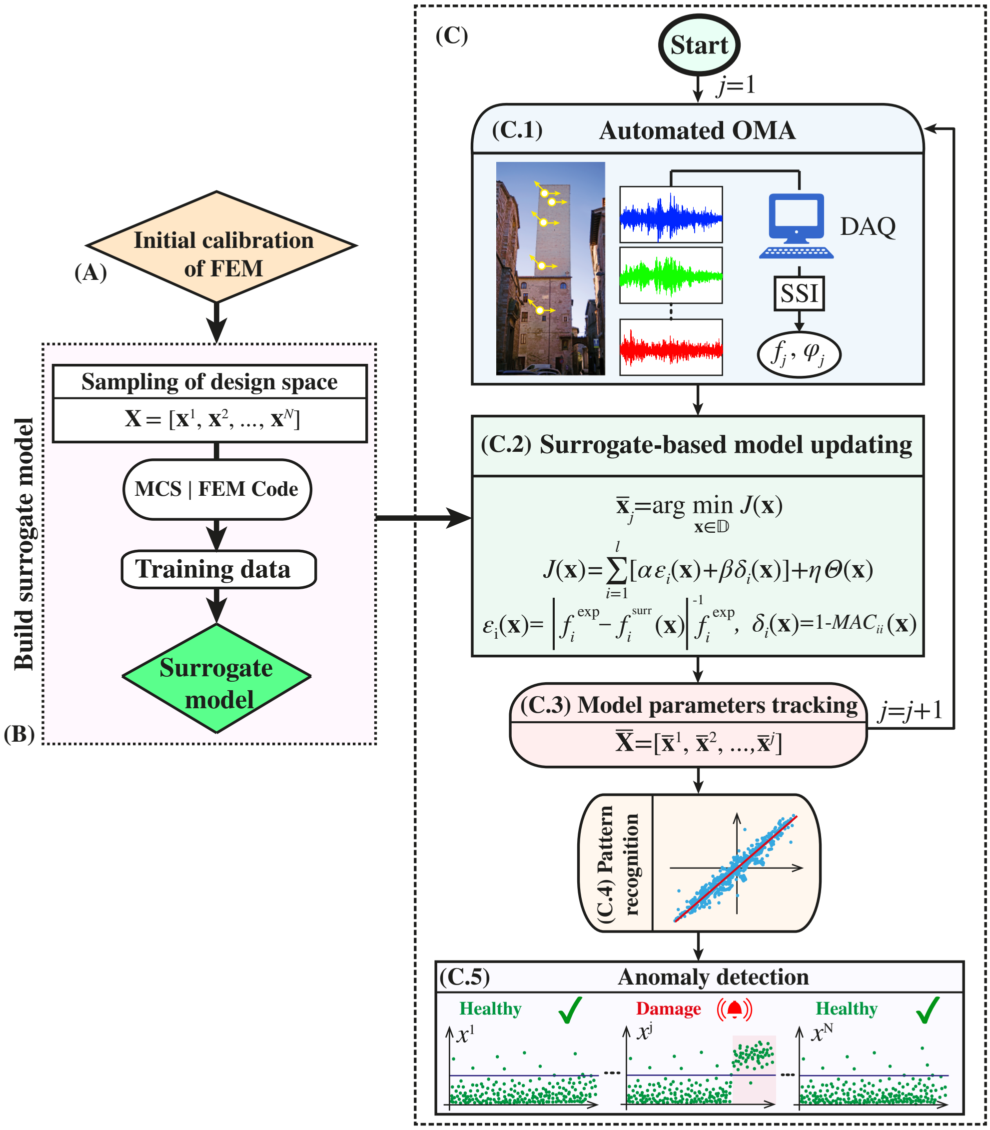

Figure 1: Flowchart of the proposed surrogate model-based continuous St-Id of historic buildings.

2.1. Surrogate modelling: Response Surface Meta-model (RSM)

The construction of a surrogate model generally comprises four consecutive steps as sketched in Fig. 2, including: (i) Selection of design variables; (ii) Sampling of the design space; (iii) Generation of the training population; and (iv) Construction of the surrogate model. The definition of the design space consists in selecting all those parameters and their variation ranges required to parametrize the original FEM and reproduce the potential damage scenarios. Let us consider m design variables $x_i \in \mathbb{R}$, $i = 1, ..., m$ (e.g. elastic properties of some structural parts) determining the response, y, of a FEM. Let us also assume that the design variables x_i are allowed to vary only within a certain physically meaningful range $[a_i, b_i]$. Accordingly, the vector of design variables $\mathbf{x}=[x_1, \ldots, x_m]^{\mathrm{T}}$ spans the m-dimensional design space $\mathbb{D} = \{\mathbf{x} \in \mathbb{R}^m : a_i \leq x_i \leq b_i\}$. To construct the surrogate model, it is necessary to assemble a training population of N individuals mapping the output y and the design space $\mathbb{D}$. This is accomplished by drawing input samples uniformly over the design space $\mathbb{D}$ and building a matrix of design sites $\mathbf{X}=[\mathbf{x}^1, \ldots, \mathbf{x}^N] \in \mathbb{R}^{m \times N}$. Then, the corresponding outputs are obtained by direct Monte Carlo simulations (MCS) using the main FEM. This allows to define an observation vector $\mathbf{Y}=[y_1, \ldots, y_N]^{\mathrm{T}}$, with $y_i \in \mathbb{R}$ being the system's response to the input $\mathbf{x}^i$.

In this work, the elastic moduli of certain regions of the FEM (referred to as macroelements hereafter) are defined as damage-sensitive input design variables, x_i, while the modal properties extracted from a linear modal analysis of the FEM are assumed as outputs. Therefore, different surrogate models must be constructed for each natural frequency and modal amplitude of all the vibration modes involved in the analysis. Specifically, if l modes of vibration are selected and n_{dof} degrees of freedom are used to characterize the mode shapes, a total of $l\,(1+n_{dof})$

surrogate models must be constructed. These include l surrogate models to represent the resonant frequencies, and $l \cdot n_{dof}$ to reproduce the modal amplitudes.

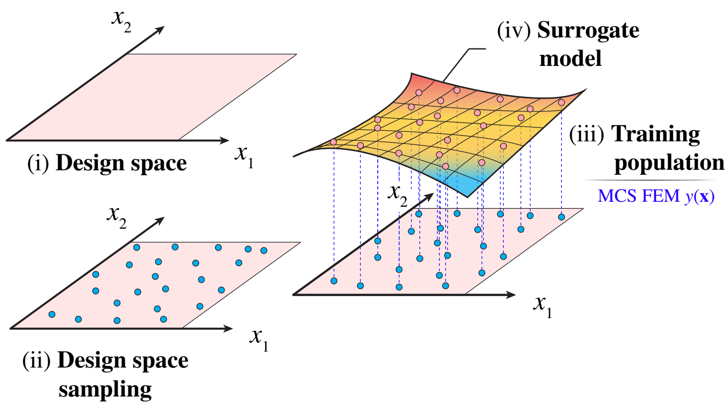

Figure 2: Schematic representation of the construction of a surrogate model over a training population.

The training population defined by the matrix of design sites $\mathbf{X}$ and the observation vector $\mathbf{Y}$ is used to construct the surrogate model. A wide variety of models can be found in the literature (see e.g. [29]), but for simplicity reasons, a second-order quadratic version of the RSM is used in this work as [8]:

$$y(\mathbf{x}) = \alpha_0 + \sum_{j=1}^{m} \alpha_j x_j + \sum_{j=1}^{m} \alpha_{jj} x_j^2 + \sum_{j=1}^{m} \sum_{i \geq j}^{m} \alpha_{ji} x_j x_i + \epsilon, \tag{1}$$

with coefficients α_0, α_j, α_{jj} and α_{ji} being the intercept, linear, quadratic, and interaction coefficients, respectively. The last term ϵ represents the error between the original FEM and the surrogate model, and it is assumed to be normally distributed with zero mean, independent, and identically distributed at each observation. The application of the model in Eq. (1) to the N individuals included in the training population can be written in matrix notation as:

$$\mathbf{Y} = \hat{\mathbf{X}}\mathbf{A} + \boldsymbol{\epsilon}, \tag{2}$$

where $\hat{\mathbf{X}}$ is an $N \times (m+1)(m+2)/2$ matrix collecting components $[1, x_j, x_j^2, x_j x_i]$ for each individual in the training population, $\mathbf{A}$ is the $(m+1)(m+2)/2$ vector of coefficients α_0, α_j, α_{jj} and α_{ji}, and $\boldsymbol{\epsilon}$ is a $(m+1)(m+2)/2$ vector of random errors. The meta-model is defined once the coefficients vector $\mathbf{A}$ is determined, which can be achieved by its least squares estimator as:

$$\mathbf{A} = \left(\hat{\mathbf{X}}^{\mathrm{T}}\hat{\mathbf{X}}\right)^{-1} \hat{\mathbf{X}}^{\mathrm{T}}\mathbf{Y}. \tag{3}$$

2.2. Surrogate model-based St-Id

In order to perform the surrogate model-based St-Id, an objective function $J(\mathbf{x})$ including the relative differences between the l target modes of vibration determined experimentally and their theoretical counterparts is introduced as follows:

$$J(\mathbf{x}) = \sum_{i=1}^{l} \left[\alpha \varepsilon_i(\mathbf{x}) + \beta \delta_i(\mathbf{x})\right] + \Theta(\mathbf{x}), \tag{4}$$

with

$$\varepsilon_i(\mathbf{x}) = \frac{\left| f_i^{\mathrm{exp}} - f_i^{\mathrm{surr}}(\mathbf{x}) \right|}{f_i^{\mathrm{exp}}}, \quad \delta_i(\mathbf{x}) = 1 - MAC_i(\mathbf{x}), \tag{5}$$

and α and β being weighting coefficients that scale the contribution of the first two terms of the objective function. Terms f_i^{exp} and $f_i^{\mathrm{surr}}(\mathbf{x})$ denote the i-th resonant frequencies obtained by OMA and the surrogate model, respectively, and MAC_i stands for the Modal Assurance Criterion (MAC) between the i-th experimental φ_i^{exp} and numerical $\varphi_i^{\text{surr}}(\mathbf{x})$ mode shapes. On this basis, the St-Id procedure is given by the following constrained non-linear minimization problem:

$$\overline{\mathbf{x}} = \arg\min_{\mathbf{x}\in\mathbb{D}} J(\mathbf{x}). \tag{6}$$

The last term in Eq. (4), $\Theta(\mathbf{x})$, represents a regularization term used to mitigate ill-conditioning limitations in the St-Id. In this work, a variation of the classical Tikhonov regularization is introduced as follows:

$$\Theta(\mathbf{x}) = \frac{1}{m}\sum_{i=1}^{m}\eta_i\frac{\left(x_i - x_i^0\right)^2}{b_i - a_i}, \tag{7}$$

where terms η_i denote trade-off parameters used to weigh the relevance of the regularization in Eq. (4) for every model parameter. The implemented regularization forces the solution to remain close to a reference vector of design variables $\mathbf{x}^0 = \left[x_1^0, ..., x_m^0\right]^{\mathrm{T}}$ or an undamaged condition. For small values of η_i, the design variable x_i remains almost unrestricted, while too large values may over-constrain the variation of x_i. It is important to remark that the aim of defining different trade-off parameters η_i for each model parameter is to tackle the particular sensitivities of the modal features to variations in the model parameters.

The modal features of the structure are experimentally obtained by automated OMA at consecutive time steps j. Therefore, the optimization in Eq. (6) is iteratively performed, and the fitted design variables are arranged in matrix form as $\overline{\mathbf{X}} = \left[\overline{\mathbf{x}}_1, ..., \overline{\mathbf{x}}_j\right]$. Such a tracking of the selected design variables provides continuous St-Id capabilities, being possible to infer the appearance of damage through the timely detection of anomalies in matrix $\overline{\mathbf{X}}$.

2.3. Statistical pattern recognition and novelty analysis

Likewise resonant frequencies, the fitting parameters in $\overline{\mathbf{X}}$ are affected by environmental and operational conditions. Hence, it is fundamental to phase out such effects through statistical pattern recognition and so unravel the activation of potential damage mechanisms in the time series of $\overline{\mathbf{X}}$. To do so, in the first place, an initial dataset of model parameters representing the healthy condition of the structure must be defined. This initial dataset, termed training period and composed of t_p data points, allows to construct a statistical model accounting for the correlations between environmental/operational conditions and the fitting parameters under healthy conditions. Such a model can be used to obtain a matrix $\widehat{\overline{\mathbf{X}}}$ of predicted fitting parameters, and afterwards assess the residuals $\mathbf{Q}$ between the original and predicted values as:

$$\mathbf{Q} = \overline{\mathbf{X}} - \widehat{\overline{\mathbf{X}}}. \tag{8}$$

Since the time series in $\widehat{\overline{\mathbf{X}}}$ solely contain the variance in the fitting parameters associated with normal operating conditions, the time series in $\mathbf{Q}$ only comprise the presence of fitting errors or new structure-environment correlations, which may indicate the appearance of damage. The residuals in $\mathbf{Q}$ throughout the training period can be assumed normally distributed with zero mean, and different in-control limits related to a certain confidence level can be set up for every fitting parameter. Hence, leveraging the direct representation of the condition of local parts of the structure by the selected fitting parameters, damage localization can be readily performed through two-class classification (damaged or undamaged) of the time series in $\mathbf{Q}$ by assessing abnormal increases in the number of outliers with respect to the afore-mentioned in-control limits.

Below a concise overview of the different techniques used in this work for estimating matrix $\widehat{\overline{\mathbf{X}}}$ is presented. These include: (a) MLR (b), PCA, and (c) ANNs.

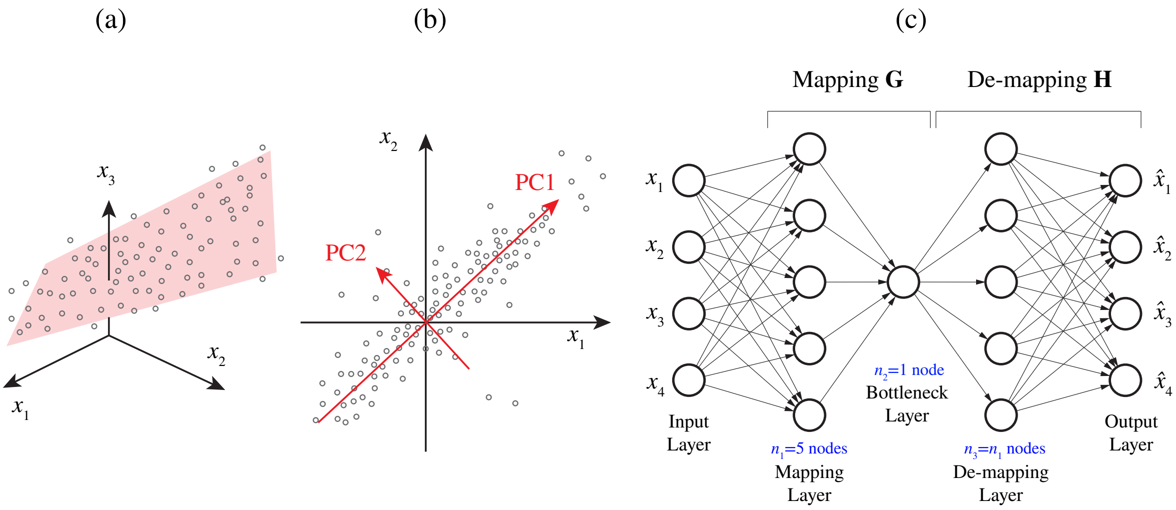

Figure 3: Statistical models used for pattern recognition of fitting model parameters: (a) MLR, (b) PCA, and (c) ANN.

(a) Multiple Linear Regression

Multiple linear regression models exploit linear correlations between the m fitting parameters and a set of p independent (explanatory) variables, called predictors, that are typically environmental and operational parameters (see Fig. 3(a)). In particular, matrix $\hat{\hat{\mathbf{X}}}$ is computed as:

$$\hat{\hat{\mathbf{X}}} = \beta \mathbf{Z}^{\mathrm{T}}, \tag{9}$$

where $\mathbf{Z} \in \mathbb{R}^{N\times(p+1)}$ is a design matrix composed of an $N \times 1$ vector of ones and an $N \times p$ matrix containing the time series of the q selected predictors, while $\beta \in \mathbb{R}^{m\times(p+1)}$ is a matrix of regression weights composed of intercept terms in the first column and linear regression coefficients in the remaining p columns. Quantities in matrix β are estimated by the least square method over the training period.

(b) Principal Component Analysis

Principal Component Analysis is a dimensionality-reduction technique used to transform databases into lower dimensional subspaces without significant losses of data variance. It starts with the projection of the original data onto the vectorial space generated by the so-called principal components (PCs) (Fig. 3(b)). Principal components are the eigenvectors of the covariance matrix of the original data, thereby PCs constitute an orthogonal basis of uncorrelated components. Ranking the PCs according to their corresponding eigenvalues (i.e. explained variance), it is possible to extract a subset of those PCs retaining most of the variance in the original data. In this work, PCs providing the largest contributions to the variance are assumed to encapsulate the effects of environmental/operational factors on the fitting variables in $\widehat{\mathbf{X}}$. In this light, matrix $\hat{\hat{\mathbf{X}}}$ can be estimated by mapping back the reduced subset of PCs onto the original data space. From a mathematical standpoint, the subspaces in PCA are defined by the eigenvectors and eigenvalues of the covariance matrix as follows:

$$\mathbf{C}_x \mathbf{U} = \mathbf{U}\mathbf{S}^2, \tag{10}$$

with $\mathbf{C}_x \in \mathbb{R}^{m\times m}$ being the covariance matrix of the original data in $\widehat{\mathbf{X}}$ normalized throughout the training period, $\overline{\mathbf{X}}_n^{tp} \in \mathbb{R}^{m\times t_p}$. The eigenvectors of $\mathbf{C}_x$ are the columns of $\mathbf{U}$ (loading matrix) and represent the PCs, and the eigenvalues are the diagonal terms of $\mathbf{S}^2$ (the off-diagonal terms are zero). The PCs are sorted in descending order according to the diagonal terms of $\mathbf{S}^2$. Geometrically, the transformed data matrix $\mathbf{T} \in \mathbb{R}^{m\times N}$ (scores matrix) is the projection of the original data ($\overline{\mathbf{X}}_n$, normalized) over the directions of the PCs in $\mathbf{U}$:

$$\mathbf{T} = \mathbf{U}^{\mathrm{T}}\overline{\mathbf{X}}_n. \tag{11}$$

It should be noted that the diagonal terms in $\mathbf{S}^2$ represent the variance contributions of each PC. By retaining only the first l columns of matrix $\mathbf{U}$ into a reduced matrix $\widehat{\mathbf{U}} \in \mathbb{R}^{m\times l}$, matrix $\widehat{\overline{\mathbf{X}}}_n$ (normalized) can be obtained as:

$$\widehat{\overline{\mathbf{X}}}_n = \left(\widehat{\mathbf{U}}\,\widehat{\mathbf{U}}^{\mathrm{T}}\right)\overline{\mathbf{X}}_n, \tag{12}$$

which enables the backward transformation from the reduced l-dimensional space of PCs to the original one. The number l of components to be retained must be chosen according to the relative contributions of the PCs to the variance in the data. If this number is too small, part of the environmental/operational effects will not be properly reproduced, while a too large value will lead to a statistical model explaining particular traits of the training period with the subsequent loss of generality.

(c) Autoassociative Neural Networks

Autoassociative neural networks, often referred to as nonlinear PCA, represent a powerful pattern recognition tool for feature extraction, dimension reduction, and novelty analysis of multivariate data [30, 31]. These consist of feedforward nets trained to produce an approximation of the identity mapping, that is, the inputs and outputs are identical and their form of learning is unsupervised. The architecture of ANNs is composed of five layers (see Fig. 3(c)): the input layer, mapping, bottleneck, demapping, and output layers. Likewise Eq. (11), ANNs seek to learn a mapping in the following form:

$$\mathbf{Y} = \mathbf{G}\left(\mathbf{X}\right), \tag{13}$$

where $\mathbf{G}$ is a non-linear vector function comprising n_2 individual functions $\mathbf{G} = \{G_1, G_2, \ldots, G_{n_2}\}$. Following an analogous approach to that in Eq. (12), the de-mapping process inversely transforms the projected data back to the original space using a second non-linear vector function $\mathbf{H}$ as:

$$\widehat{\overline{\mathbf{X}}} = \mathbf{H}\left(\mathbf{Y}\right). \tag{14}$$

Vector functions $\mathbf{G}$ and $\mathbf{H}$ are computed by minimizing the Euclidean norm of the differences between the fitted design variables and the estimates by the ANN (i.e. with minimum loss of information). Arbitrary non-linear functions $y = g(x)$ are sought by ANNs in the following general form:

$$y_k = \sum_{j=1}^{n_2} w_{jk}^2\, h\left(\sum_{i=1}^{n_1} w_{ij}^1\, x_i + b_j\right), \tag{15}$$

where y_k and x_i are the k-th and i-th components of y and x, respectively, w_{ij}^k denotes the weight factor between the i-th node in the k-th layer and the j-th node in the successive layer, and b_j is a node bias. The term n_i indicates the number of nodes in the i-th layer, and the transfer function $h(x)$ is a continuous and monotonically increasing function with the output range from 0 to 1.

The complexity of the ANNs chiefly depends upon the number of nodes in the mapping layers (n_1, n_3), while the bottleneck one is usually defined as a low-dimensional layer ($n_1, n_3 > n_2$). Too few nodes in the mapping layers may compromise the accuracy of the neural network, while too many mapping nodes may lead to over-learning of the stochastic content of the data rather than the underlying driving sources. In this work, neural networks with $n_1 = 5$, $n_2 = 1$ and $n_3 = 1$ neurons have been utilized as shown in Fig. 3(c). The ANNs have been trained using the fitting model parameters obtained throughout the training period and the Levenberg-Marquardt backpropagation algorithm, and sigmoidal transfer functions have been employed in all the hidden layers as well as the output layer.

3. Application case study: The Sciri Tower in Perugia, Italy

This section presents the case study of the Sciri Tower. Specifically, the details of the structure and its modal identification through continuous OMA are firstly presented in Sections 3.1 and 3.2, respectively. There follows the modelling of the structure in Sections 3.3 and 3.4. It is important to remark that the quality of the metamodel of the Sciri Tower, which is the main outcome of this study, depends upon both the quality of the large-scale FEM and the construction of the surrogate model itself. Thus, to guarantee the quality of the resulting metamodel, model calibration is performed first at the large-scale FEM level in Section 3.3 through first-order sensitivity analysis and a GA. Afterwards, details of the construction of the surrogate model and its quality assessment are reported in Section 3.4.

3.1. *The Sciri tower*

In order to validate the proposed damage identification procedure, a historic masonry civic tower located in the historical centre of Perugia in Italy (Figure 4 (a)), named *Torre degli Sciri*, is selected as a case study. The tower is 41 m high, has a rectangular cross-section (7,15 x 7,35 m), and is made of white limestone masonry. Up to the first 17 m, the tower is inserted into a building ensemble with approximate cross-section dimensions of 20 x 25 m. This medieval tower has been the subject of study in several investigations by the authors, so interested readers may refer to references [28, 29, 32, 33] for further information about its architecture.

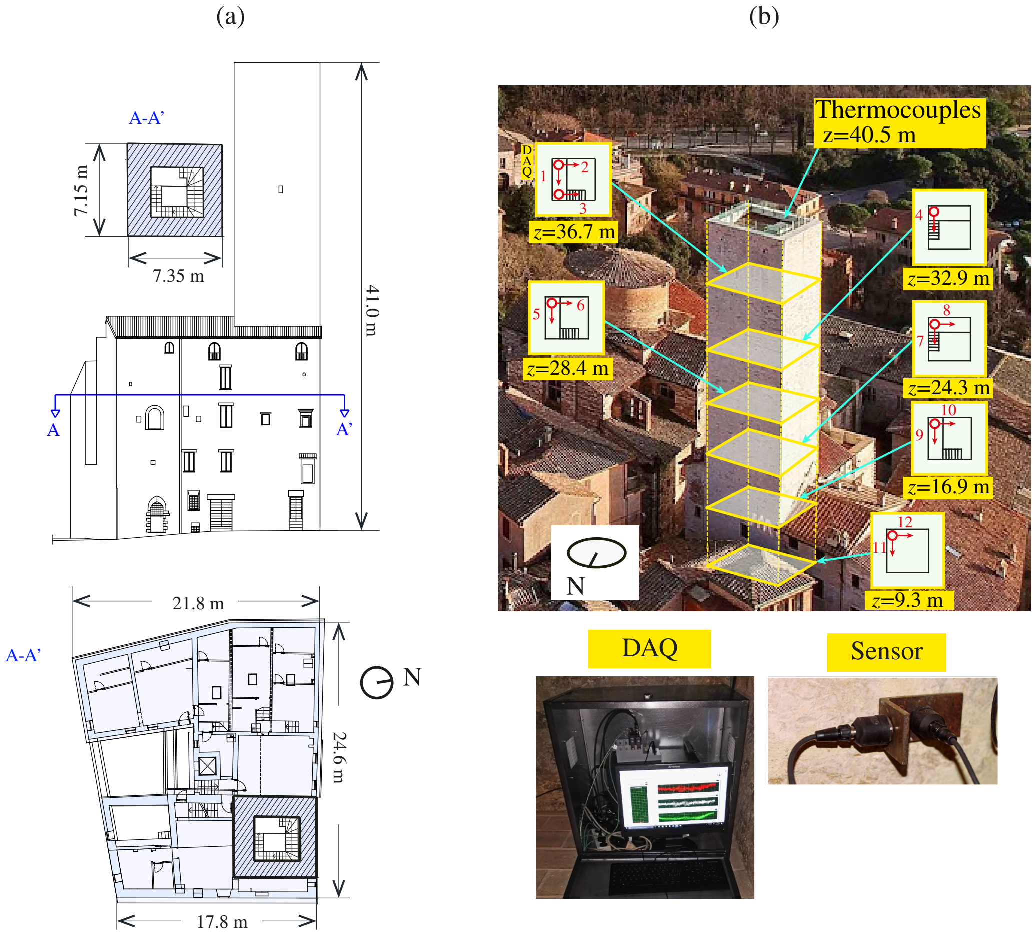

Figure 4: Elevation and plan views (a), and sensors layout for continuous monitoring of the Sciri Tower (b).

3.2. *Dynamic monitoring and modal identification*

A continuous environmental/dynamic monitoring campaign with a relatively large number of sensors was performed from February 13th until March 10th 2019. As shown in Fig. 4 (b), twelve high sensitivity (10 V/g) uniaxial accelerometers model PCB 393B12 were installed at six different heights of the tower, acquiring ambient vibrations at a sampling frequency of 1652 Hz and down-sampled to 40 Hz. Two K-type thermocouples were also installed at the level z = 40.5 m to measure indoor and outdoor temperatures at a sampling frequency of 0.4 Hz. The modal identification of the tower was continuously performed using 30-min long acceleration records via two in-house codes recently developed by the authors and reported in reference [34]. This pair of software codes, named MOVA and MOSS, provide all the necessary tools for the management of long-term integrated SHM systems. These include specific toolboxes for signal preprocessing, automated OMA, frequency tracking, data fusion of heterogeneous monitoring data, and novelty analysis through the use of statistical process control charts. In particular, the Covariance-driven Stochastic Subspace Identification (COV-SSI) method was used to identify the modal properties of the Sciri Tower. This method is suitable for the identification of linear structures under white-noise excitations, which are the common conditions assumed in AVT of historic constructions. Readers interested in OMA under non-stationary excitations may refer to works on Independent component analysis (ICA) methods (see e.g. [35, 36]). The parameters used in the identification included maximum and minimum numbers of block rows/columns in the Toeplitz matrix of covariances of 140 and 200, respectively, with steps of 5, and model's orders running from 40 to 80 with steps of 2. Seven vibration modes have been identified in the frequency range between 0 and 10 Hz as shown in Fig. 5: two flexural modes in NW direction (Fx1 and Fx2), two flexural modes in SW direction (Fy1 and Fy2), one torsional mode, Tz1, and two higher order flexural modes, Fx3, Fy3. Table 1 collects the identified resonant frequencies, damping ratios, and modal phase collinearity (MPC) values exploiting the first 30-min acceleration records acquired in the tower. The MPC values of all the modes are above 95% (classically damped), except for modes Fx2 and Fy2 where values of 84.9% and 80.2% are obtained, which indicates that the latter are non-classically damped or the level of excitation is insufficient to correctly identify these modes.

Table 1: Experimentally identified natural frequencies f_i^{exp}, damping ratios ζ_i and Modal Phase Collinearity (MPC) estimated through COV-SSI on 13th February 2019 at 14:00 UTC.

Mode	f_i^{exp} [Hz]	ζ_i [%]	MPC_i [%]
Fx1	1.692	0.918	99.8
Fy1	1.891	0.779	99.4
Fx2	5.539	3.066	84.9
Fy2	5.829	2.175	80.2
Tz1	8.205	1.783	99.8
Fx3	9.795	1.365	98.9
Fy3	10.820	3.166	95.2

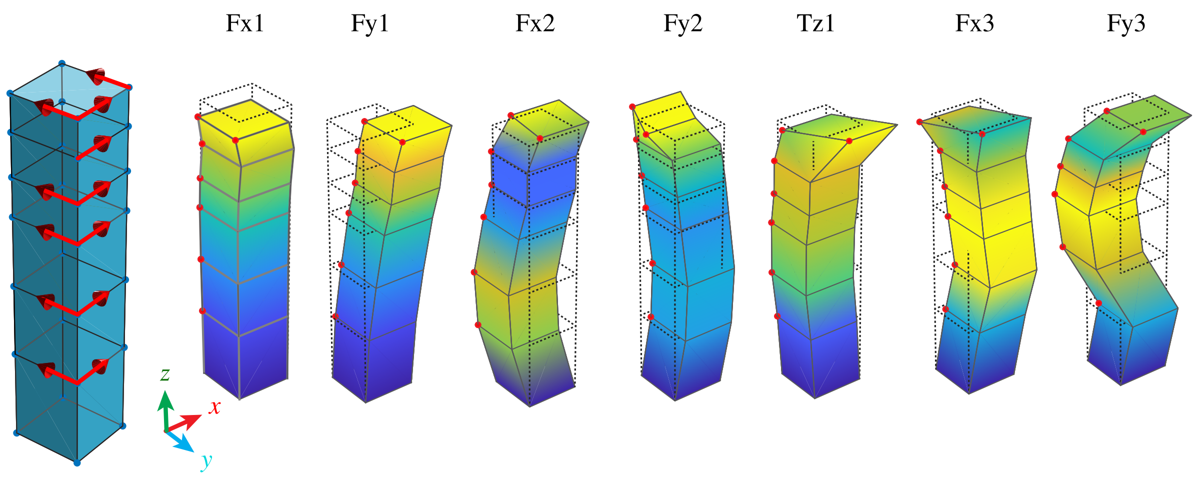

Figure 5: Experimentally identified mode shapes of the Sciri Tower using the vibration data acquired on 13th February 2019 at 14:00 UTC.

Figure 6 reports the tracking of the modes of vibration of the Sciri Tower. It is noted that the afore-mentioned modes of vibration are consistently found throughout the complete monitoring period. In this figure, it is observed that modes Fx1, Fy1, Tz1, and Fy3 exhibit quite stable behaviours with average (MAC,MPC) values of (1.00,99.35), (1.00,98.42), (1.00,99.32), (0.99,96.87), and (0.99,97.61), respectively. Such high MPC values indicate that these modes are well excited and their mode shapes are essentially real. Therefore, these modes can be consistently modelled using the classical Rayleigh damping model. Differently, modes Fx2 and Fy2 have mean (MAC,MPC) values of (0.92,81.94) and (0.93,79.88), respectively. According to the previous results from Table 1, these modes are eminently complex with constantly low MPC values and show no apparent correlation with the level of ambient excitation. This may indicate the existence of damping mechanisms for these modes that cannot be assimilated to a proportional damping model, possibly due to soil-structure interaction phenomena. Further analyses in this regard are left for future research, and the results in Fig. 6 justify the exclusion of the mode shapes of modes Fx2 and Fy2 in the subsequent surrogate model-based St-Id.

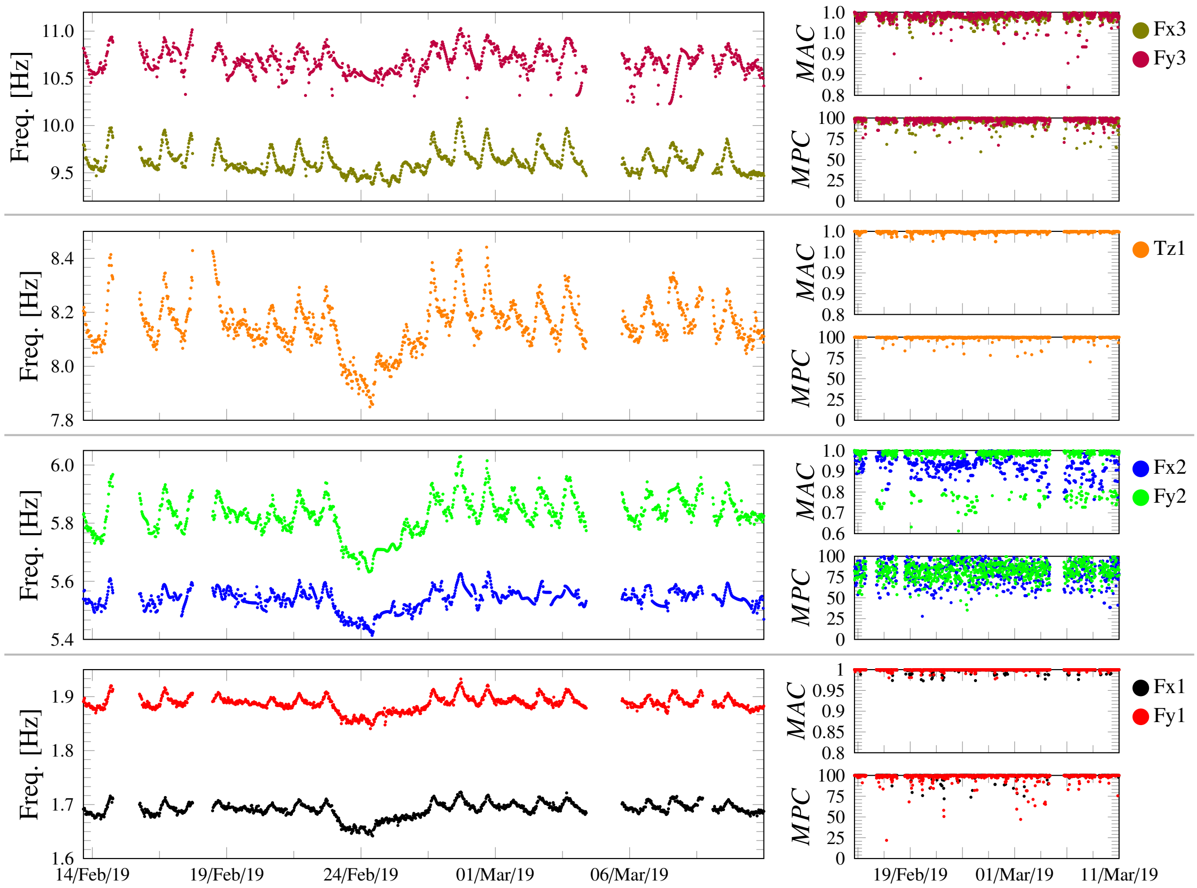

Figure 6: Tracking of the modes of vibration of the Sciri Tower since February 13th until March 10th 2019.

3.3. FEM of the Sciri Tower and initial calibration using a genetic algorithm

As the basis for the ensuing surrogate model, a fully detailed 3D FEM of the building ensemble of the Sciri Tower has been built using the commercial software ABAQUS 6.10 (see Fig. 7). The geometry of the model has been created according to existing architectural drawings and in-situ geometry surveys. Fixed translational boundary conditions have been defined at the ground level, and the material model of the masonry has been considered as elastic isotropic with Young's modulus $E = 4.04$ GPa, Poisson's ratio $\nu = 0.25$, and mass density $w = 2.20$ t/m^3 according to the Italian technical standard for square stone masonry. The geometry has been meshed using ten-node tetrahedral elements `C3D10` with mean element size of about 34 cm, leading to a total number of elements and nodes of 157069 and 685147, respectively. It is important to remark that a simplified building-tower connection through spring elements was initially attempted. Nevertheless, such an approach failed to reproduce some of the experimentally identified modes, in particular the torsional one Tz1. To overcome these limitations, a detailed modelling of the adjoining buildings as shown in Fig. 7 became imperative, which entailed a substantial increase in the computational burden of the resulting model. Therefore, the present case study constitutes an excellent example of the need for computationally efficient surrogate models to perform model-base damage identification.

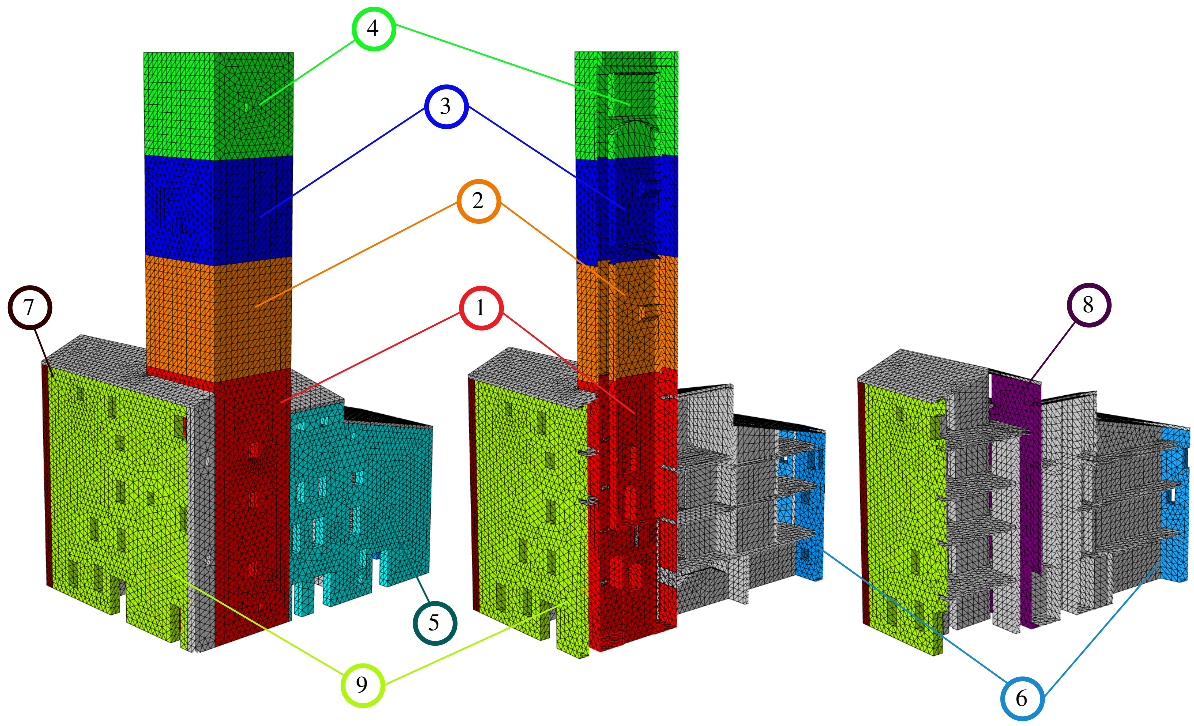

Figure 7: FEM of the Sciri Tower and geometry partitioning for model updating using a GA.

Afterwards, in order to obtain theoretical modal estimates consistent with the experimental ones, a two-step calibration of the FEM has been carried out. Firstly, a preliminary calibration has been performed using first-order sensitivity analysis. To do so, the model has been partitioned into eighteen different regions with distinct material properties, differentiating the tower, ten masonry walls, four floors, and three parts of the roof of the building aggregate. Their elastic moduli and mass densities have been tuned using the modal features extracted from the first vibration data acquired on February 13$^{\text{th}}$ 2019. Secondly, the material properties of the building ensemble have been further calibrated using a GA. Nine different sections of the building (labelled from 1 to 9 in Fig. 7) with material properties exhibiting largest sensitivities have been selected for the calibration. Specifically, fifteen different material parameters of the afore-mentioned sections, including Young's moduli and mass densities, have been included in the calibration through a GA as reported in Table 2. Genetic algorithms are a global search method for non-linear optimisation based upon the Darwin's theory of evolution [37]. The GAs proceed by taking populations of individuals or solutions, whose fitness values are evaluated by the objective function to be maximized/minimized. The best individuals of each generation are selected to produce the next one through crossover and mutation operators, and the process is repeated until an user-defined maximum number of iterations or fitness tolerance is reached. In this work, populations of 45 individuals have been sequentially drawn considering a range of variation of ±15% with respect to their initial values (first column in Table 2), and the cost function in Eq. (4) has been used as the fitness function ($\alpha = 1, \beta = 1, \eta_i = 0$). The optimal set of model parameters determined after several iterations are presented in Table 2, and the comparison of the numerical and experimental modal properties is reported in Table 3. Note that the initial (uncalibrated) properties in Table 2 are those obtained in the previous calibration step through sensitivity analysis. Good agreements can be observed for modes Fx1, Fy1, Tz1, Fx3 and Fy3 with relative differences in terms of resonant frequencies below 5% and MAC values above 0.8. Conversely, considerably small MAC values are noted for modes Fx2 and Fy2, specially the latter one with a value of 0.084. In these cases, the reason for such a low similarity between the numerical and experimental mode shapes is ascribed to the high complexity of modes Fx2 and Fy2 reported previously in Table 1 and Fig. 6. The accuracy achieved in Table 3 is considered sufficient for the aim of the present work, and further analyses deepening into possible soil-structure interaction are left for future research.

Table 2: Mechanical parameters of the FEM of the Sciri Tower before and after the initial calibration by GA (subscripts relate the corresponding quantity to the FEM partitions shown in Fig. 7).

Param.	Uncalibrated	Calibrated
E_1 [GPa]	5.77	5.14
E_2 [GPa]	5.77	5.80
E_3 [GPa]	5.77	6.63
E_4 [GPa]	5.77	6.22
E_5 [GPa]	0.90	0.98
E_6 [GPa]	160.00	137.53
E_7 [GPa]	0.95	0.86
E_8 [GPa]	1.90	1.76
E_9 [GPa]	0.70	0.68
$\rho_1 = \rho_2$ [t/m^3]	2.20	1.93
$\rho_3 = \rho_4$ [t/m^3]	2.20	2.31
ρ_6 [t/m^3]	1.60	1.71
ρ_7 [t/m^3]	2.20	2.53
ρ_8 [t/m^3]	2.20	2.52
ρ_9 [t/m^3]	1.90	1.85

Table 3: Comparison between experimental and numerical modal parameters after the initial calibration by GA.

	Resonant frequencies [Hz]					MAC values	
Mode	Exp.	Uncalibrated	Rel. Diff. [%]	Calibrated	Rel. Diff. [%]	Uncalibrated	Calibrated
Fx1	1.692	1.754	-3.700	1.692	-0.017	0.972	0.976
Fy1	1.891	1.967	-4.009	1.886	0.259	0.960	0.965
Fx2	5.539	5.770	-4.167	5.591	-0.941	0.798	0.757
Fy2	5.830	6.196	-6.273	6.166	-5.760	0.107	0.084
Tz1	8.205	8.005	2.433	7.900	3.720	0.871	0.850
Fx3	9.795	9.894	-1.012	9.654	1.445	0.907	0.934
Fy3	10.819	10.858	-0.359	10.864	-0.415	0.781	0.846

3.4. Surrogate model construction

In order to construct the surrogate model of the Sciri Tower, the previously calibrated FEM has been parametrized through a set of damage-sensitive design variables. In particular, the FEM has been subdivided into four partitions or macro-elements M_i, $i = 1, ..., 4$, as shown in Fig. 8. Similarly to sections 1 to 4 in Fig. 7, macro-elements M_1, M_2, M_3 and M_4 comprise the portions of the building located between heights of 0-18.9 m, 18.9-26.8 m, 26.8-33.8 m, and 33.8-41.0 m, respectively. Note that, differently from section 1 in Fig. 7, macro-element M_1 also includes the adjoining building. According to this partition, the Young's modulus E_i of all the elements contained in a generic macro-element M_i has been defined as a random variable as:

$$E_i = E_i^0 (1 + k_i), \tag{16}$$

with E_i^0 being the initial value of the Young's modulus of the elements contained in the i-th macro-element. Parameters k_i denote linear proportionality coefficients of the elastic moduli of macro-elements M_i, and represent the design variables $\mathbf{x} = [k_1, k_2, k_3, k_4]^{\mathrm{T}}$ in the surrogate model-based damage identification approach previously introduced in Section 2.2. In virtue of this parametrization, permanent reductions in one of the components of $\mathbf{x}$ would indicate the presence of damage in the corresponding macro-element.

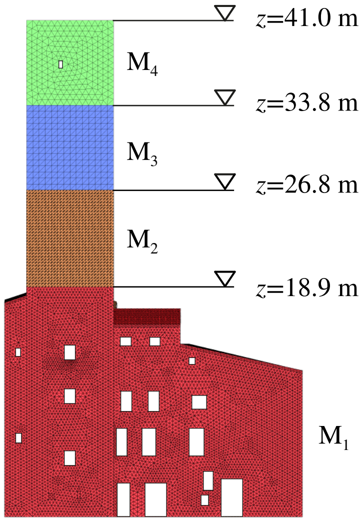

Figure 8: Partitioning of the FEM of the Sciri Tower into macro-elements M_i, $i = 1, ..., 4$.

The surrogate model previously introduced in Section 2.1 is constructed on the basis of a training population generated by Monte Carlo simulations of the 3D FEM. To this end, the design space formed by k_i, $i = 1, ..., 4$, must be uniformly sampled in the first place. The stiffness coefficients k_i have been defined as random variables with upper/lower bounds of ±15%, which are assumed to cover the range of expected variations in the elastic moduli of macro-elements M_i. Thereby, the design space $\mathbb{D}$ in Eq. (6) takes the form of:

$$\mathbb{D} = \left\{ \mathbf{x} \in \mathbb{R}^4 : -0.15 \leq k_i \leq 0.15 \right\}. \tag{17}$$

With the purpose of ensuring the homogeneous representation of the design space, random samples have been drawn uniformly over $\mathbb{D}$ using an iterative Latin hypercube sampling method with 20 iterations to maximize the minimum distance between samples. An optimal population size of 512 individuals has been determined through a convergence analysis similar to the one carried out in our previous work [29]. Figure 9 shows the statistical analysis of the drawn up training population. Note in this figure that the histograms of the design variables k_i, $i = 1, ..., 4$, are almost flat, which demonstrates the uniformity of the sampling of $\mathbb{D}$. The analysis is further extended in Fig. 10 where the probability density functions (PDFs) of the resonant frequencies (a) and the histograms of the MAC values (b) of the target natural modes are depicted.

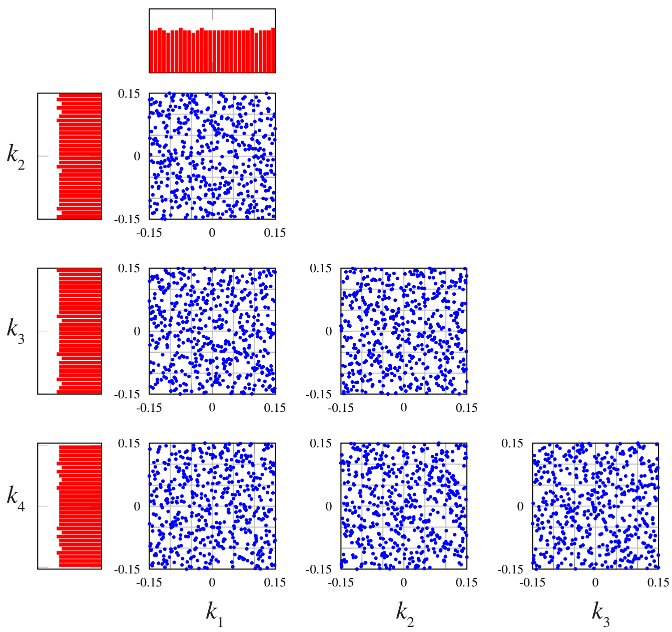

Figure 9: Statistical analysis of training population (512 individuals) of the design variables k_i, $i = 1, ..., 4$.

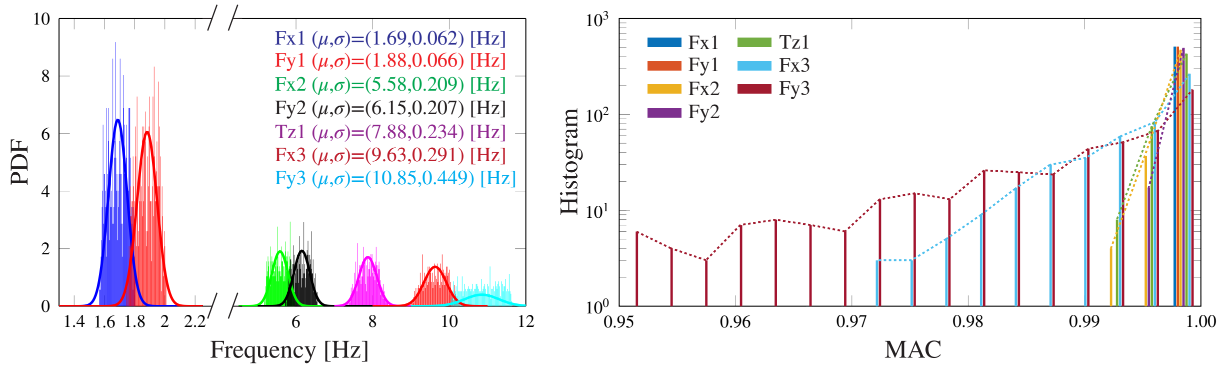

Figure 10: (a) Probability density functions (PDFs) of the resonant frequencies, and (b) histograms of the MAC values of the first seven natural frequencies obtained with the FEM of the Sciri Tower (training population of 512 individuals).

Figure 11 shows a scatter plot describing the relationship between the resonant frequencies of the Sciri Tower predicted by the original FEM and the surrogate model. The low scatter of the points around the diagonal line corroborates that the surrogate model is formed with accuracy.

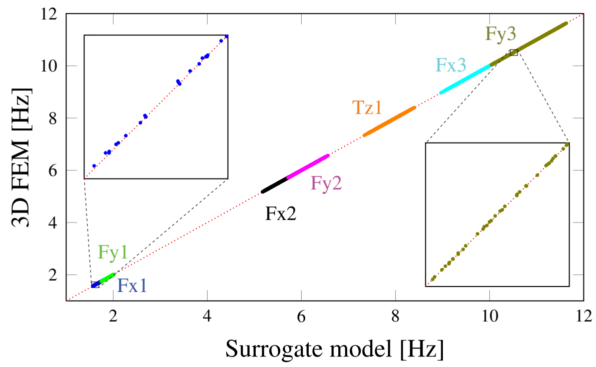

Figure 11: Scatter plot of resonant frequencies predicted by the 3D FEM versus those predicted by the surrogate model of the Sciri Tower.

4. Simulation of earthquake-induced damage scenarios through non-linear incremental analysis

With the purpose of validating the proposed damage identification approach, different earthquake-induced damage scenarios have been simulated through a displacement-controlled pushover analysis. This consists in a static-nonlinear analysis where the building is subjected to gravity loading and an increasing lateral displacement along the NW direction applied at the topmost floor of the tower. The lateral load increases continuously through elastic and inelastic behaviour until an ultimate condition is reached. In order to reproduce the non-linear mechanical behaviour of the masonry, the classic Concrete Damage Plasticity (CDP) constitutive model [38] has been used. This approach, proposed by Lubliner *et al*. [39] and then modified by Lee and Fenves [40], is well-suited for the modelling of brittle masonry under cyclic loading considering cracking in tension and crushing in compression. Given the lack of characterization tests of the masonry of the tower, the non-linear mechanical properties assigned to the FEM have been estimated from the literature as shown in Table 4. During the analysis, the shear base forces, top displacements, and tensile damage parameters d_t have been monitored. The tensile damage parameter d_t denotes the material degradation, and spans from 0 (undamaged material) to 1 (total loss of strength). Figure 12 furnishes the monitored base shear force versus top displacements. Seven different damage scenarios, labelled from (a) to (g) in Fig. 12, are defined with increasing top displacements of 0.0 cm, 1.0 cm, 2 cm, 3.36 cm, 4.5 cm, 7 cm and 13 cm, respectively. The damage patterns in terms of contour maps of damage parameters d_t are represented in the right hand side of Fig. 12. The main failure mechanism consists of a major shear crack originating at approximately the mid height of the SE façade when the upper part of the tower reaches a maximum displacement of 3.36 cm (damage scenario (d)). This diagonal crack propagates downward until it reaches the NW façade, completely losing its bearing capacity and causing its subsequent collapse. This occurs when the maximum top displacement reaches a value of 13 cm (g), when convergence issues impede the continuation of the FEM simulation. Some other secondary cracking patterns can be observed in the intermediate damage scenarios (c), (c) and (e) as a result of stress concentrations at openings and the loss of connection with the adjoining building in the SE façade of the tower. These seven different scenarios allow to validate the proposed surrogate model-based damage identification approach and to appraise its sensitivity and reliability as reported in the upcoming sections.

Table 4: Mechanical parameters utilized in the CDP model for masonry.

Elasto-plastic behaviour		**Tensile behaviour**		
K_c[a]	0.667	Tensile stress σ_t [kN/m^2]	Cracking strain $\tilde{\varepsilon}_t^{ck}$ [-]	Tensile damage parameter d_t [-]
Eccentricity	0.10	160	0.00E-00	0.00
Viscosity parameter[b]	0.003	120	1.74E-04	0.55
Dilation angle [°]	21	84	3.77E-04	0.80
		16	7.59E-04	0.90

[a] K_c is the ratio of the second stress invariant on the tensile meridian.
[b] The viscosity parameter is used for the viscoplastic regularization of the constitutive equations.
* Compressive strength σ_c = 3500 kN/m^2

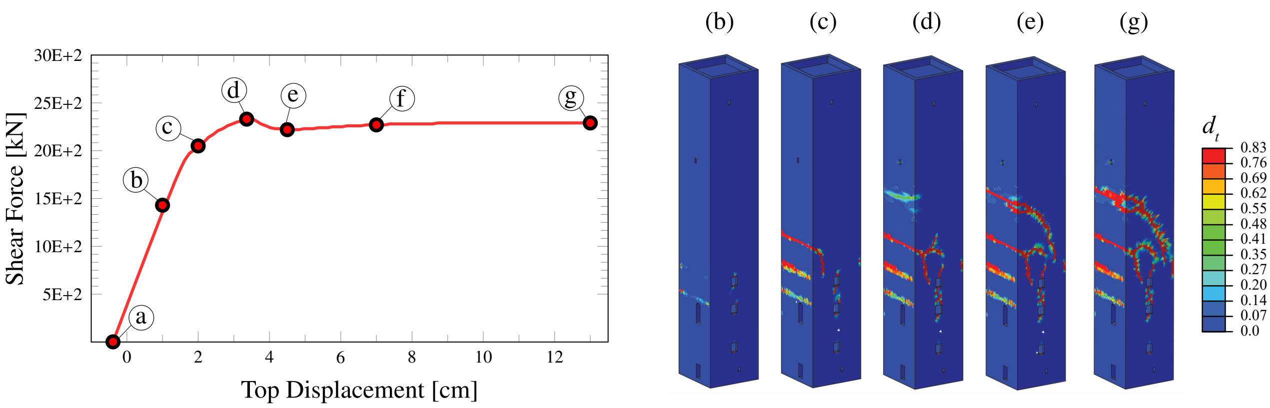

Figure 12: Base shear force versus top displacement curve obtained by displacement-controlled pushover analysis of the Sciri Tower and simulated crack patterns in the tower.

In order to include the simulated damage scenarios from Fig. 12 into the time series of modal features (resonant frequencies and mode shapes) extracted during the vibration testing campaign reported in Section 3.2, every damage stage in Fig. 12 (from (a) to (g)) has been characterized through a non-linear modal analysis. This consists in releasing the imposed lateral displacement in the model when the corresponding maximum displacement is achieved, and performing the eigenvalue/eigenvector analysis related to modal analysis considering the tangent stiffness matrix of the FEM. This leads to the results reported in Fig. 13 where the frequency decays and MAC values of the first seven modes of vibration are plotted against top displacement. It is interesting to note that sudden drops are found in terms of MAC values when the top displacement reaches a value of about 3.36 cm (c), that is when the major failure mechanism in the tower activates. This corresponds to a drift ratio of 1.52‰ in the free standing portion of the tower.

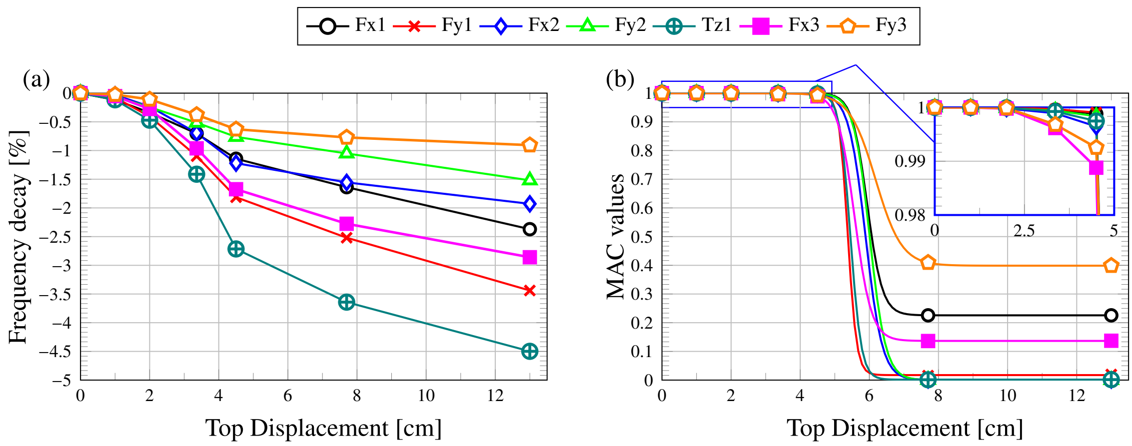

Figure 13: Frequency decays (a) and MAC values (b) of the first seven modes of vibration obtained by the displacement-controlled pushover analysis of the FEM of the Sciri Tower. The continuous lines in (b) are obtained by fitting sigmoid functions through non-linear least squares.

5. Continuous surrogate model-based St-Id for automated damage localization

In this section, the effectiveness and reliability of the proposed surrogate model-based damage identification approach is appraised for the case study of the Sciri Tower. To do so, the weighting parameters α and β in the cost function in Eq. (4) have been defined as 1 and 0.5, respectively. The trade-off parameters η_i included in the regularization term $\Theta(\mathbf{x})$ in Eq. (7) have been tuned after the initial sensitivity analysis furnished in Fig. 14. This figure represents the sensitivity of the modal features of the 3D FEM in terms of resonant frequencies (S^f_{ij}) and mode shapes (S^φ_{ij}) to variations in the design parameters k_i. These sensitivity coefficients S_{ij}, $i = 1, ..., 4$, $j = 1, ..., 7$, have been computed through a perturbation analysis as:

$$S^f_{ij} = \frac{\Delta f_j}{\Delta k_i}, \quad S^\varphi_{ij} = \frac{1 - \Delta MAC_{jj}}{\Delta k_i}, \tag{18}$$

with Δ denoting the finite difference operator. While in classic model updating the least sensitive parameters are typically excluded from the optimization or clustered together with other design parameters, such an approach would imply here the impossibility to locate damage in certain regions of the structure. In this particular case study, the low sensitivity of the modal features of the Sciri Tower to variations in k_4 considerably hinders the location of damage in M_4. In order to accommodate the different sensitivities reported in Fig. 14, and as an attempt to keep the damage localization capabilities in M_4, larger trade-off parameters η_i are assigned to design variables with larger sensitivities and vice versa. In particular, after some manual tuning iterations, good results have been obtained assuming $\eta_1 = 1$, $\eta_2 = 0.5$, $\eta_3 = 0.25$, and $\eta_4 = 0.15$.

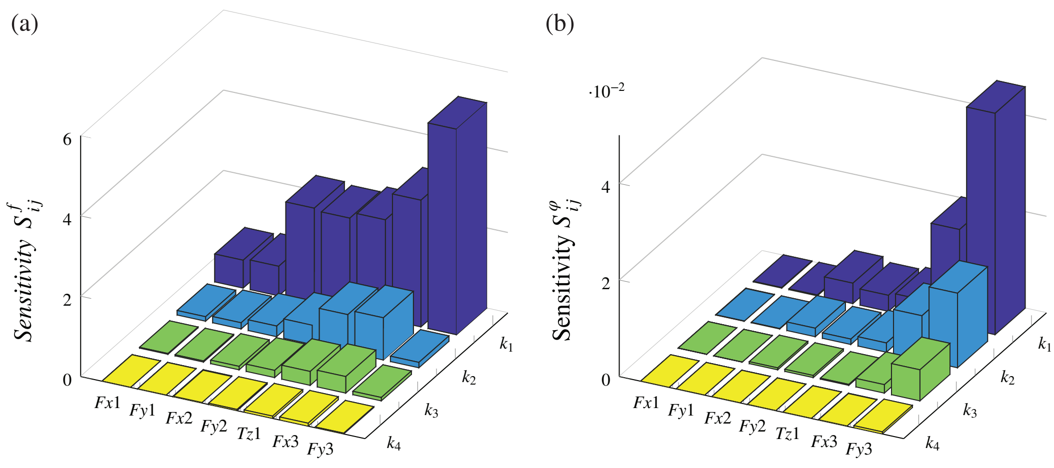

Figure 14: Sensitivity coefficients of the modal properties predicted by the 3D FEM of the Sciri Tower in terms of resonant frequencies (S^f_{ij}) (a) and mode shapes (S^φ_{ij}) (b) to variations in the design variables k_i.

The proposed surrogate model-based approach has been applied to perform the online St-Id of the Sciri Tower. Based upon the dynamic identification results reported in Fig. 6, the St-Id has been performed continuously for each set of identified modal data (30 min) over the testing period since February 13th until March 10th 2019. To this aim, the non-linear minimization problem in Eq. (6) has been iteratively solved using a Particle Swarm optimization algorithm. A reference vector of design variables $\mathbf{x}^0 = [0, 0, 0, 0]^T$ has been considered (i.e. $\mathbf{x}^0$ represents the situation when macro-elements M_i possess nominal values of Young's modulus), along with a parameter variation range of $-0.15 \leq k_i \leq 0.15$. The mode shapes of modes Fx2 and Fy2 have been excluded from the optimisation because of their high complexity level as previously reported in Table 1. To do so, the term $\delta_i(\mathbf{x})$ in Eq. (4) is forced to take the value of $\delta_i(\mathbf{x}) = 1$ for these modes. In order to assess the consequences of including or not the mode shapes in the St-Id, two sets of weighting coefficients α and β have been considered, namely $[\alpha, \beta]$=[1,0.5] and $[\alpha, \beta]$=[1,0] (i.e. disregarded mode shapes). The outcome of the continuous surrogate model-based St-Id is presented in Fig. 15. Let us recall that macro-element M_1 is constituted by different materials, all of them affected by the design variable k_1. Nonetheless, for clarity purposes, only the elastic moduli E_i corresponding to the sections of the tower according to the partition in Fig. 8 are reported herein. It is interesting to note in Fig. 15 that the proposed approach can capture daily fluctuations in the intrinsic stiffness of the tower. Specifically, increasing and decreasing trends of E_i can be observed during daytime and night-time, respectively. With regard to the consequences of exploiting mode shapes in the St-Id, it is evident from Fig. 15 that the time series obtained using $\beta = 0$ exhibit a considerably larger amount of outliers. This fact evidences limitations in the St-Id due to ill-conditioning in the optimization problem. Conversely, when $\beta = 0.5$, the solution is further constrained by the term $\delta_i(\mathbf{x})$ in $J(\mathbf{x})$ (Eq. (6)), leading to quite clear time series of identified Young's moduli. In this case, the time series of E_2, E_3, and E_4 are sorted in decreasing order, indicating that the stiffness of the tower decreases in height, which is consistent with the architectural configuration of the tower. The smallest values are found for E_1, although it is not straightforward to extract conclusions about the intrinsic stiffness of the tower here since the building aggregate and the bottom section of the tower are clustered together into macro-element M_1. One essential aspect regards the computational times required to perform the St-Id. While the 3D FEM takes on average a CPU time of 10 min to complete one single linear modal analysis in a standard PC (64-bit, 64 GB RAM, Intel Xeon processor E3-1225 v5, 3.30 GHz CPU), the St-Id of the Sciri Tower using the RSM only requires 0.02 s (i.e. a reduction of 99.998%). Such a low evaluation time allows to perform the St-Id in about 0.3 s, making the proposed approach fully compatible with real-time SHM applications.

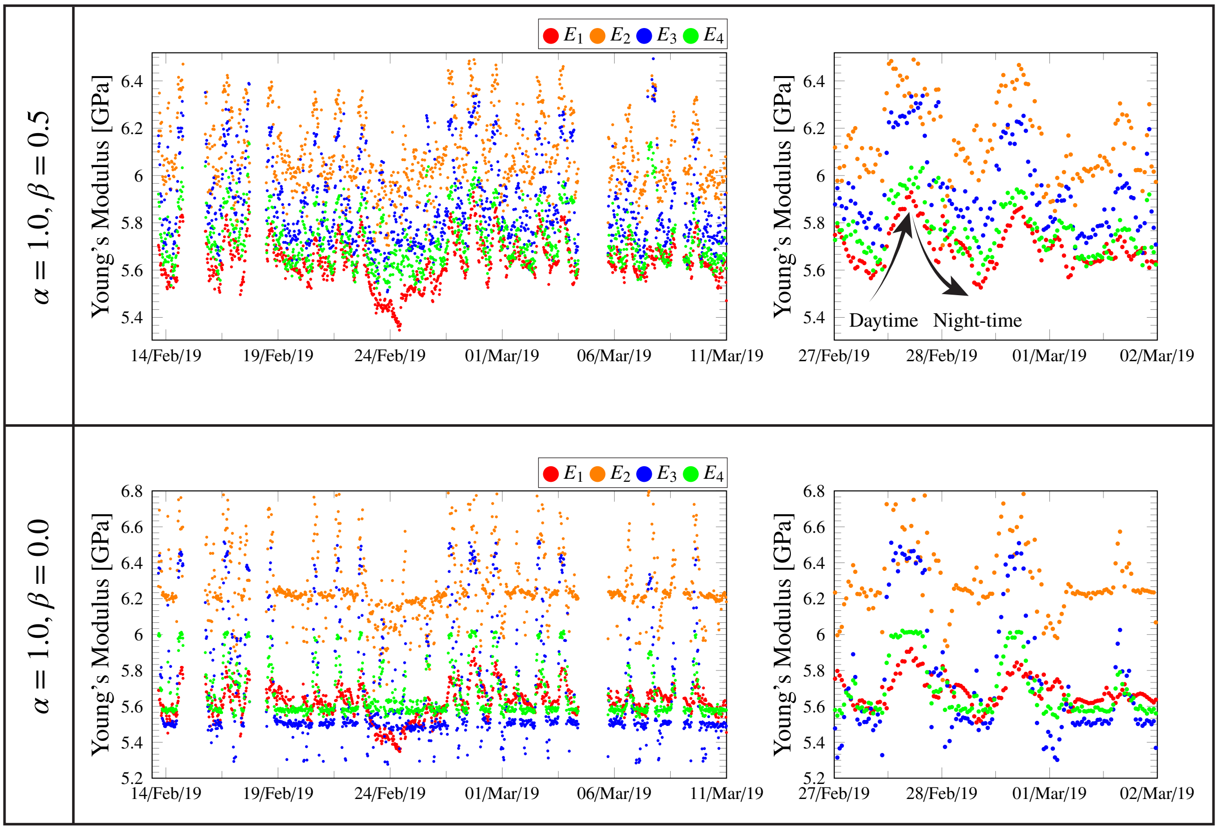

Figure 15: Time series of fitted Young's moduli of macro-elements M_i, $i = 1, ..., 4$, enabled by the online surrogate model-based St-Id of the Sciri Tower.

The effect of the mean environmental temperature on the identified Young's moduli is further analysed in Fig. 16. The correlations are investigated through linear least squares regression over the time series of E_i after a cleansing process. The latter consists in the detection of corrupting outliers in the time series with the purpose of extracting a cleansed database from which robust statistics can be extracted. The process starts with the application of the Minimum Covariance Determinant (MCD) method [41] to find a sample subset providing a robust estimation of the covariance matrix. The MCD method seeks a sample subset within a multivariate dataset (in this work the identified Young's moduli E_i) that minimize the covariance matrix. Specifically, we have sought a subset of $\approx 0.9n_p$ samples, with n_p being the number of data points in the time series of E_i (1057 data samples). Then, the samples in the time series of E_i are ranked according to the Mahalanobis distance with respect to the previously defined sample subset, and those with distances larger than twice the standard deviation of the Mahalanobis distances are identified as outliers. On this basis, the correlations indicated in Fig. 16 have been obtained disregarding the identified outliers (data points denoted with empty circle markers). In view of these results, a positive correlation between E_i and environmental temperature can be observed in all the cases. That is to say, the structure behaves in a stiffer manner during the day, while the overall stiffness decreases during the night. Such a behaviour agrees with the daily fluctuations also observed in the time series of tracked resonant frequencies from Fig. 6. This is also consistent with previously reported results in the literature on vibration-based SHM of masonry structures (see e.g. [17, 42]). This behaviour is usually ascribed to the closure of superficial cracks, micro-cracks or minor discontinuities in the structure induced by thermal expansion. Interestingly, the proposed surrogate model-based St-Id approach further allows to explore the local sensitivities of intrinsic stiffness to thermal variations. It can be noted in Fig. 16 that temperature sensitivities decrease with height. This behaviour can be also understood as a result of the closure of micro-cracks induced by thermal expansion, which presumably causes a stronger effect on those regions of the structure where expansion is more constrained, that is, close to the base and where the material is more heterogeneous. Conversely, the macro-elements of the upper part of the tower are more free to expand and the contribution of thermally-induced crack closure to the effective stiffness is less influential.

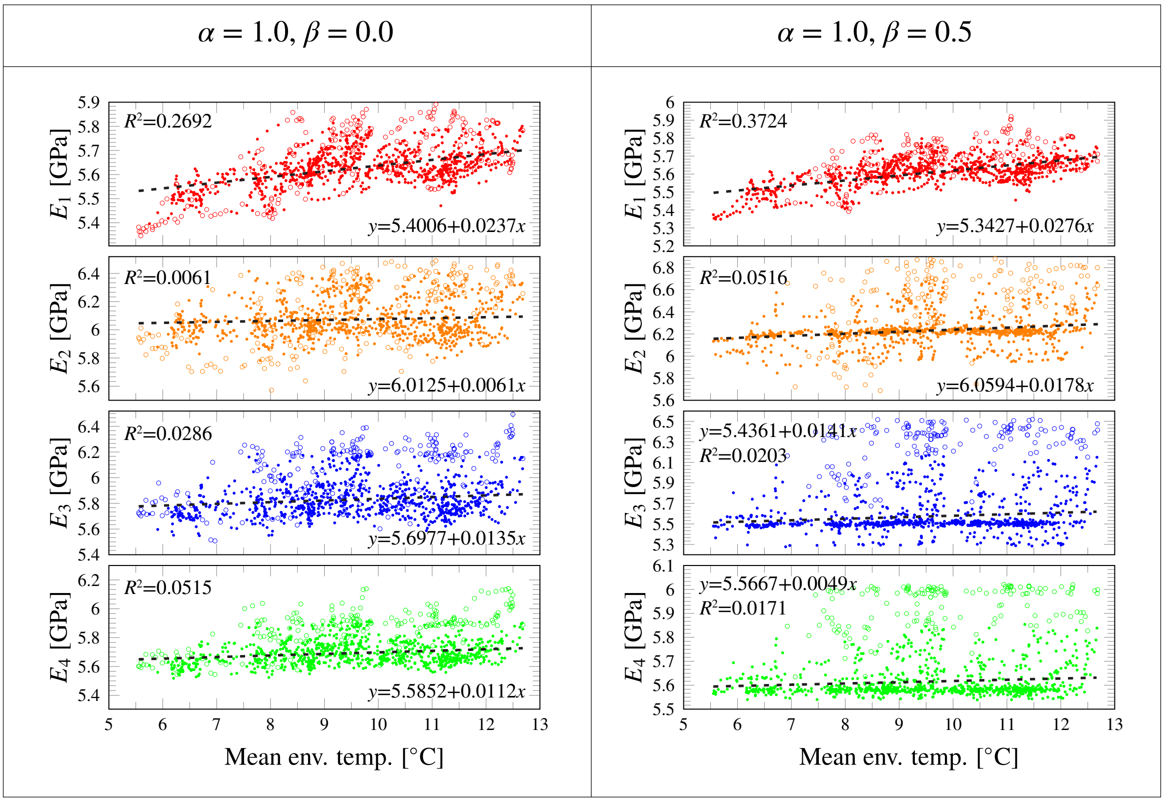

Figure 16: Correlations between the identified Young's moduli of macro-elements M_i, $i = 1, ..., 4$, of the Sciri Tower and the mean environmental temperature. Empty circle markers denote identified outliers in the time series.

Figure 17 shows the time series of identified elastic moduli E_i along with the predicted ones adopting the statistical models previously introduced in Section 2.3, namely MLR, PCA, and ANN. In the case of PCA, one single PC sufficed to explain more than 90% of the variance in E_i. A training period of two weeks and a half (800 data points) has been set up to construct the statistical models. Additionally, Fig. 17 also depicts the histograms of the residuals Q_i between the identified moduli E_i and the predicted ones $\hat{E}_i$, i.e. $Q_i = E_i - \hat{E}_i$. With the purpose of assessing the effectiveness of the different models, Table 5 reports the statistical analysis of the residuals in Fig. 17. In this figure, it can be observed that PCA and ANN yield closer estimates to the identified E_i compared to MLR, which can be further verified by the standard deviation values of the residuals in Table 5. Another important aspect to be appraised concerns the statistical distribution of residuals. Since a proper statistical model must reproduce most of the variance caused by environmental factors (e.g. temperature, humidity or wind), the residuals must approximately follow a Gaussian distribution with zero mean and standard deviation mainly determined by identification errors and noise sources. In order to check whether the statistical distributions of residuals in Fig. 17 can be produced by a Gaussian distribution, different statistics are presented in Table 5, including kurtosis, skewness, and the Kolmogorov-Smirnov (KS) statistic. The KS test is commonly used to decide whether a sample can be generated by a certain statistical distribution, in this case a Gaussian distribution. It can be noted in Table 5 that the KS test only accepts the null hypothesis (the data are normally distributed) in the case of the time series of E_1 and E_2 predicted by MLR (with a confidence level of 95%, i.e. $KS \geq 0.05$). The reason for this is ascribed to the limited duration of the training period, which unfortunately could not be extended because of logistic issues. Despite exhibiting superior capabilities for unveiling non-linear correlations, the PCA and ANN models achieve worse representations of the underlying variance sources in the time series of E_i compared to MLR, which is possibly due to the limited number of observations in the training period. Conversely, although larger residuals are obtained when using MLR, the fact that this model relies on the main source of variance as a predictor (the environmental temperature) makes it achieve more normally distributed residuals.

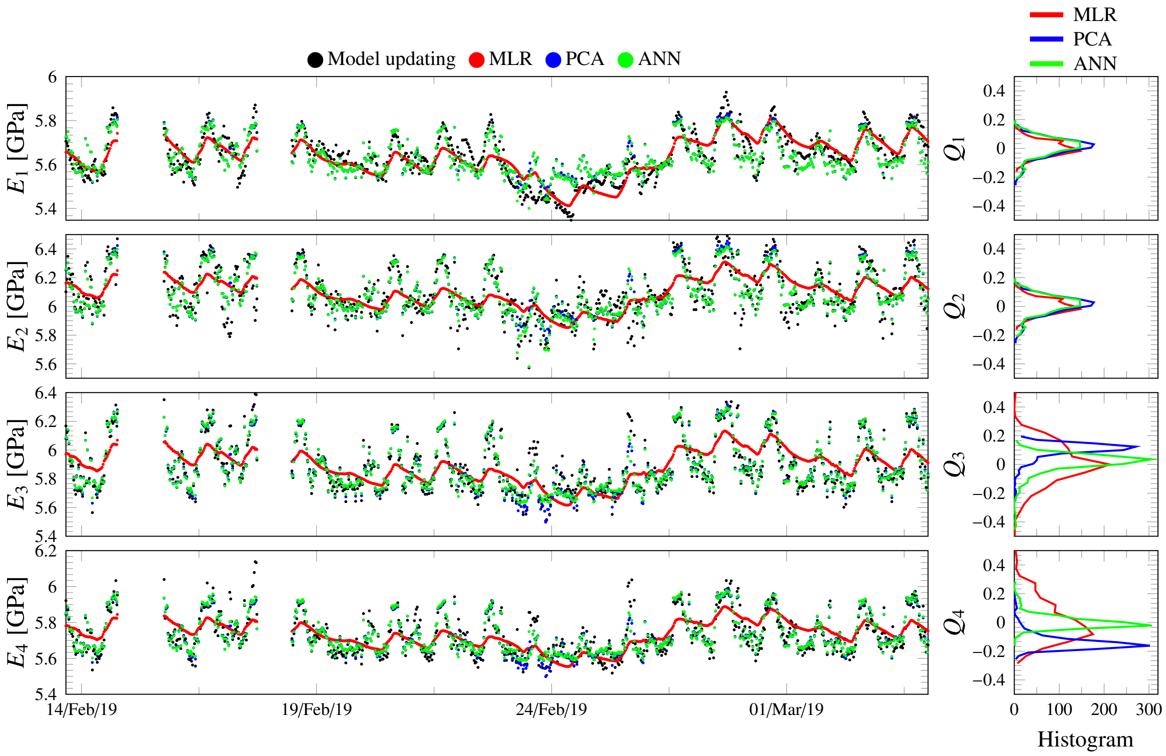

Figure 17: Identified elastic moduli E_i of the Sciri Tower and predicted time series using MLR, PCA and ANN, along with the histograms of their residuals.

Table 5: Statistical analysis results of the residuals between identified elastic moduli E_i of the Sciri Tower and the values predicted by the MLR, PCA and ANN models.

		$\alpha = 1, \beta = 0.5$			$\alpha = 1, \beta = 0.0$		
		MLR	PCA	ANN	MLR	PCA	ANN
Q_1	Mean [GPa]	0.00	0.00	0.01	0.00	0.01	0.01
	STD [GPa]	0.06	0.07	0.07	0.05	0.08	0.08
	Kurtosis	3.09	4.19	3.60	3.25	3.96	3.83
	Skewness	0.01	-0.83	-0.66	-0.07	-0.45	-0.51
	KS*	0.77	0.00	0.00	0.30	0.00	0.00
Q_2	Mean [GPa]	0.01	0.00	0.01	0.01	0.01	0.02
	STD [GPa]	0.14	0.07	0.07	0.18	0.09	0.09
	Kurtosis	4.03	10.58	11.76	4.41	8.95	9.15
	Skewness	0.14	-2.20	-2.25	0.45	-2.11	-1.49
	KS*	0.17	0.00	0.00	0.00	0.00	0.00
Q_3	Mean [GPa]	0.01	0.00	0.00	0.01	0.00	0.00
	STD [GPa]	0.15	0.04	0.05	0.26	0.04	0.05
	Kurtosis	5.16	9.66	7.91	3.15	9.67	9.00
	Skewness	1.09	2.08	1.64	0.67	2.23	1.58
	KS*	0.00	0.00	0.00	0.00	0.00	0.00
Q_4	Mean [GPa]	0.01	0.00	0.00	0.00	0.00	0.00
	STD [GPa]	0.09	0.04	0.04	0.11	0.04	0.03
	Kurtosis	4.97	7.87	6.59	3.29	5.94	7.06
	Skewness	1.11	1.63	1.36	0.86	1.54	1.31
	KS*	0.00	0.00	0.00	0.00	0.00	0.00

**Kolmogorov-Smirnov statistic*

Finally, Fig. 18 presents the damage identification results using the proposed approach for the simulated damage scenarios previously reported in Section 4. The effects of the considered damage scenarios have been included in the time series of experimentally identified modal features after the training period from the 7$^{\text{th}}$ March 2019 in terms of frequency decays and damaged mode shapes (reported in Fig. 13). In this light, Fig. 18 depicts the squared values of the residuals of the elastic moduli of macro-elements M_i throughout the monitoring period. Moreover, upper control limits (UCL) are indicated with red dashed horizontal lines to ease the identification of permanent variations in the statistical distributions of the residuals. These UCLs have been defined as four times the standard deviation of the residuals within the training period ($UCL_i = 4\sigma_i^p$). From these results, it is quite evident that outliers concentrate in macro-element M_2, which agrees well with the damage patterns previously discussed in Fig. 12. Additionally, some outliers can be also recognized in macro-element M_1, while almost no outliers are noted in the last two macro-elements M_3 and M_4.

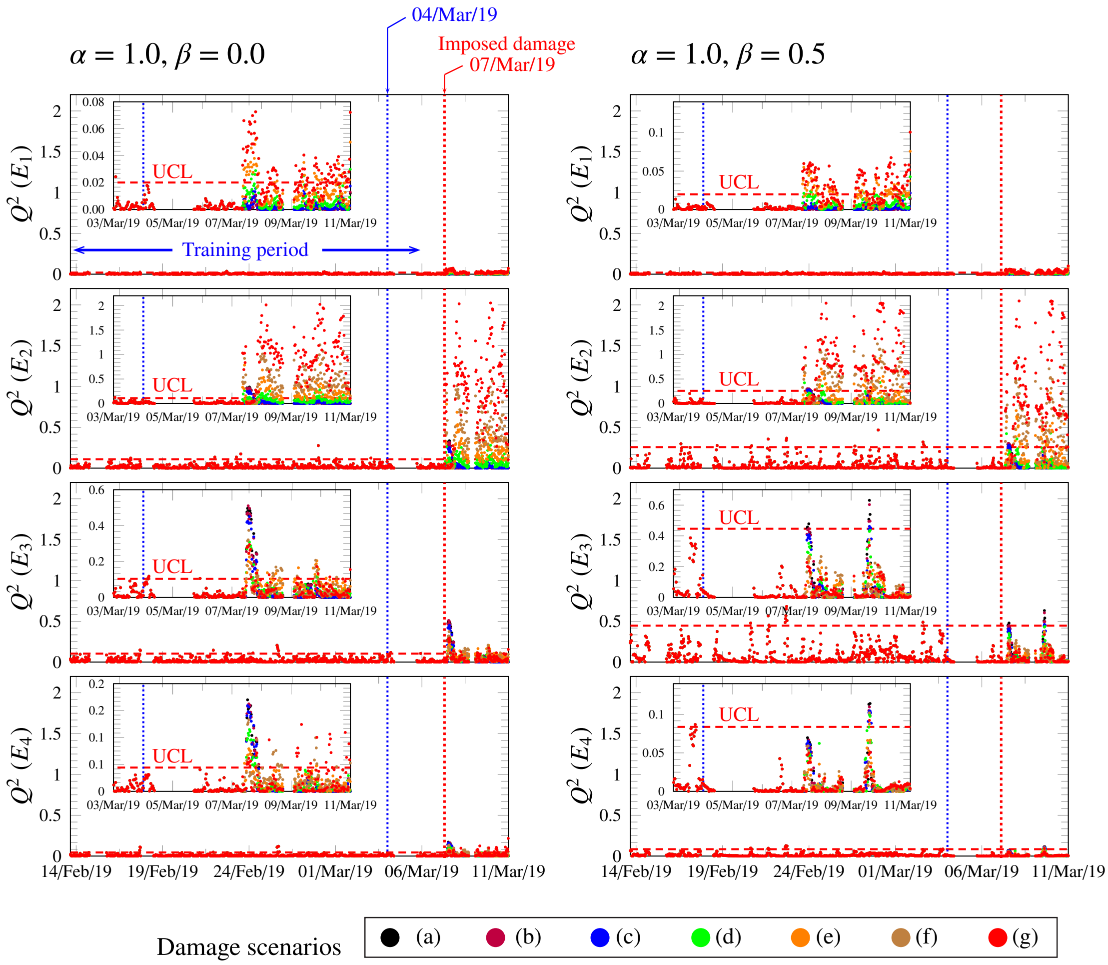

Figure 18: Results of surrogate model-based damage identification of the Sciri Tower when subjected to simulated damage scenarios with increasing severity (training population = 900 individuals, $UCL_i = 4\sigma_i^p$).

In order to devise suitable metrics for determining whether the structure may experience damage, as well as to shed some light into the importance of including or not mode shapes in the optimization, Figs. 19 and 20 report the analysis of outliers in the time series from Fig. 18. Specifically, the number of outliers (data points exceeding the UCL) after the training period are plotted in Fig. 19 against the simulated damage scenarios when using MLR, PCA, and ANN. From these analyses, it can be concluded that the best results are achieved when using the MLR model and including the mode shapes in the optimization ($\beta = 0.5$). In this case, increases in the number of outliers are concentrated in macro-elements M_1 and M_2, which agrees with the simulated damage patterns. Moreover, almost no variations are observed in the number of outliers for macro-elements M_3 and M_4 where no damage is expected. Interestingly, when mode shapes are not included in the optimization, no significant increases in the number of outliers are detected until the damage scenario (d), that is when the major diagonal crack in the tower takes place. These results demonstrate the usefulness of including mode shapes into the surrogate model-based St-Id to minimize ill-conditioning limitations and enable early-stage damage localization. Considerably worse results are obtained with the two other statistical models, where a considerable amount of outliers is also found for macro-elements M_3 and M_4 which are known to remain healthy. The reason for this poor performance is ascribed to the limited number of data samples in the training period, hence larger databases would be required to further appraise their effectiveness. These analyses are completed with the results furnished in Fig. 20, where deviations in the distributions of outliers are studied. For this purpose, a damage index is defined as the the ratio between the average values of the squared residuals outside and inside the training period. It is noted that the best damage identification results are again those obtained using the MLR model and including mode shapes in the St-Id (β = 0.5). In this case, the proposed damage index exhibits a monotonically increasing behaviour with the damage severity, outputting largest values for the macro-element M_2, followed by the macro-element M_1, and constant values close to zero in the case of macro-elements M_3 and M_4 where no damage is expected. These results demonstrate the ability of the proposed surrogate model-based approach for damage identification, being capable of localizing structural pathologies and quantifying their severity through novelty analysis of the time series of tracked model parameters.

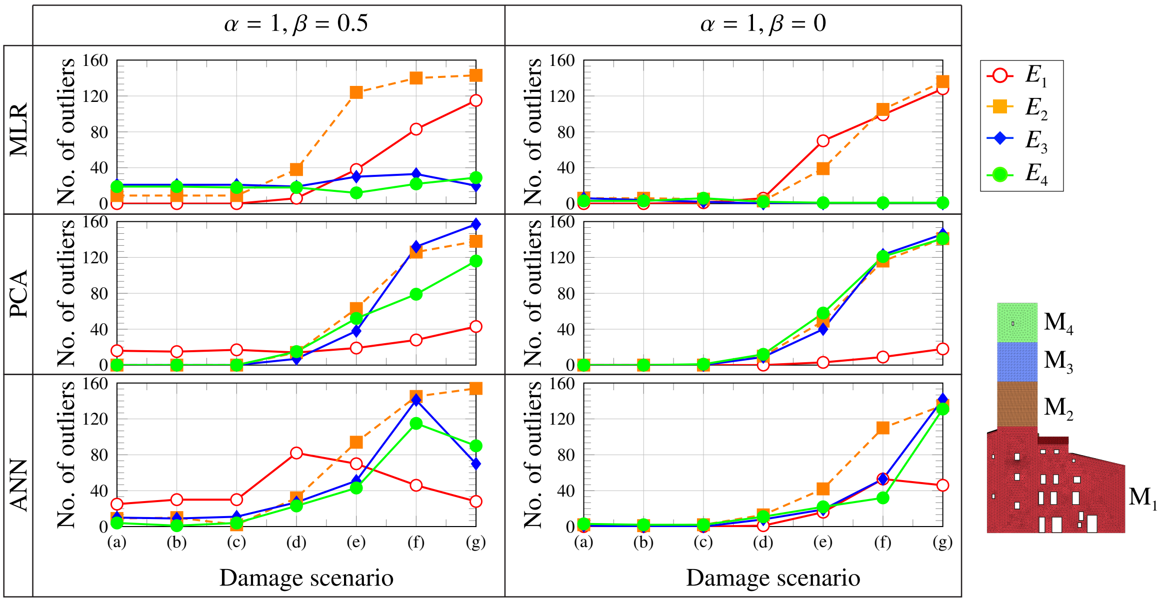

Figure 19: Damage identification results in the Sciri Tower through outlier counting in the time series of residuals between identified Young's moduli and statistical predictions (training population = 900 individuals, $\mathrm{UPC}_i = 4\sigma_i^p$).

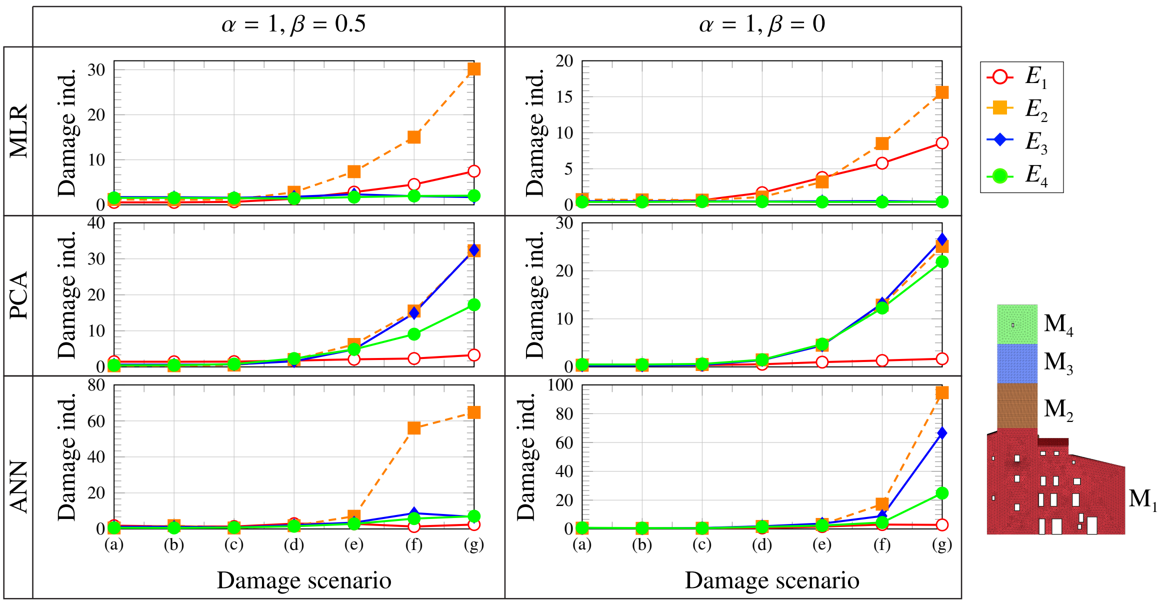

Figure 20: Damage identification results in the Sciri Tower through outlier analysis of residuals between identified Young's moduli and statistical predictions. The damage index is defined as the ratio between the average values of the squared residuals outside and within the training period (training population = 900 individuals).

6. Conclusions

This paper has presented a metamodel-based pattern recognition approach for real-time identification of earthquake-induced damage in historic masonry structures. The proposed methodology consists in the continuous St-Id of the structure under study through a computationally inexpensive RSM. The surrogate model bypasses a fully detailed 3D FEM of the structure, and certain model parameters are identified in real time by minimizing the mismatch between theoretical estimates and experimentally identified modal features by automated OMA. A newly proposed regularization term is included in an objective function accounting for both resonant frequencies and mode shapes. The proposed regularization is a variation of the classical Tikhonov regularization where different penalty functions are assigned to every model parameter. Specifically, larger trade-off factors are imposed to those model parameters exhibiting larger sensitivities and vice versa. This attempts to minimize ill-conditioning limitations in the associated optimization problem, as well as to accommodate differential parameter sensitivities with the aim of preserving damage localization capabilities all throughout the structure. Damage localization is achieved through pattern recognition and novelty analysis of the time series of continuously identified model parameters. For this purpose, environmental effects are phased out by applying different statistical models constructed over a training/baseline dataset characterizing the healthy state of the structure. The case study of the Sciri Tower located in the city of Perugia (Italy) has been presented to validate the effectiveness of the proposed approach. The modal features of the tower have been continuously assessed with an environmental/dynamic SHM system installed since February 13th until March 10th 2019. In order to appraise the effectiveness/reliability of the proposed approach, different earthquake-induced damage scenarios with increasing severities have been investigated by conducting nonlinear static/modal incremental analyses of the 3D FEM of the tower. The reported results have demonstrated the suitability of the proposed approach for damage identification (detection, localization, and quantification), and pave the way for the development of superior long-term vibration-based SHM systems with real-time damage identification capabilities. The key contributions of this work can be summarized as follows:

- Mode shapes are minimally affected by environmental factors, and their inclusion into the optimization problem associated with the St-Id is crucial for minimizing ill-conditioning limitations and achieving accurate damage identification results. Furthermore, it has been shown that the proposed regularization is capable of limiting ill-conditioning while accommodating differential model parameter sensitivities, thus preserving damage identification capabilities throughout the structure.

- The use of the RSM makes the proposed methodology completely compatible with real-time SHM systems, demanding CPU times of about 0.3 s in the case study of the Sciri Tower.

- The presented results have demonstrated that the proposed methodology can unveil the effects of environmental factors upon the local stiffness of structures. It has been shown that the correlations between the intrinsic structural stiffness and the underlying driving environmental factors can be unravelled by applying standard pattern recognition techniques to the time series of continuously identified model parameters.

- The damage identification capabilities of the proposed methodology have been appraised using simulated earthquake-induced damage scenarios with increasing severity. Seven different damage scenarios have been characterized through non-linear incremental analyses of a 3D FEM of the Sciri Tower, and included into the time series of experimental modal features in the shape of frequency decays and damaged mode shapes obtained by nonlinear modal analysis.

- The reported results have demonstrated that damage can be identified through novelty analysis of the residuals between the time series of fitted model parameters and the predictions of a regression model constructed from a baseline/training database. Accurate results have been obtained when using the MLR model with environmental temperatures (outdoor and indoor) as predictors and including mode shapes in the St-Id. Two different metrics based upon outliers analysis have been proposed to assess the localization and severity of damage, namely outliers counting and deviation analysis of the statistical distribution of residuals.

Acknowledgements

This work was supported by the Italian Ministry of Education, University and Research (MIUR) through the funded project of national interest "DETECT-AGING - Degradation Effects on sTructural safEty of Cultural heriTAGe constructions through simulation and health monitorING" (Protocol No. 201747Y73L).

References

[1] J. S. Mitchell, From vibration measurements to condition-based maintenance: Seventy years of continuous progress, Sound and Vibration (magazine) 41 (1) (2007) 62–79.

[2] S. W. Lin, T. H. Yi, H. N. Li, L. Ren, Damage detection in the cable structures of a bridge using the virtual distortion method, Journal of Bridge Engineering 22 (8) (2017) 04017039. doi:10.1061/(ASCE)BE.1943-5592.0001072.

[3] P. Cawley, Structural health monitoring: Closing the gap between research and industrial deployment, Structural Health Monitoring 17 (5) (2018) 1225–1244. doi:10.1177/1475921717750047.

[4] K. Liu, N. E. G., Ontology-based semi-supervised conditional random fields for automated information extraction from bridge inspection reports, Automation in Construction 81 (2017) 313–327. doi:10.1016/j.autcon.2017.02.003.

[5] P. Hüthwohl, R. Lu, I. Brilakis, Multi-classifier for reinforced concrete bridge defects, Automation in Construction 105 (2019) 102824. doi:10.1016/j.autcon.2019.04.019.

[6] T. H. Yi, H. N. Li, M. Gu, A new method for optimal selection of sensor location on a high-rise building using simplified finite element model, Structural Engineering and Mechanics 37 (6) (2011) 671–684. doi:10.12989/sem.2011.37.6.671.

[7] H. S. Park, B. K. Oh, Real-time structural health monitoring of a supertall building under construction based on visual modal identification strategy, Automation in Construction 85 (2018) 273–289. doi:10.1016/j.autcon.2017.10.025.

[8] I. Venanzi, A. Kita, N. Cavalagli, L. Ierimonti, F. Ubertini, Continuous OMA for Damage Detection and Localization in the Sciri tower in Perugia, Italy, in: Proceedings of the 8th International Operational Modal Analysis Conference (IOMAC), Copenhagen, Denmark, 2019, 2019.

[9] Y. An, E. Chatzi, S. H. Sim, S. Laflamme, B. Blachowski, J. Ou, Recent progress and future trends on damage identification methods for bridge structures, Structural Control and Health Monitoring 26 (10) (2019) e2416. doi:10.1002/stc.2416.

[10] L. J. Sánchez-Aparicio, Á. Bautista-De Castro, B. Conde, P. Carrasco, L. F. Ramos, Non-destructive means and methods for structural diagnosis of masonry arch bridges, Automation in Construction 104 (2019) 360–382. doi:10.1016/j.autcon.2019.04.021.

[11] D. Bru, S. Ivorra, M. Betti, J. M. Adam, G. Bartoli, Parametric dynamic interaction assessment between bells and supporting slender masonry tower, Mechanical Systems and Signal Processing 129 (2019) 235–249. doi:10.1016/j.ymssp.2019.04.038.

[12] P. Pachón, M. Infantes, M. Cámara, V. Compán, E. García-Macías, M. I. Friswell, R. Castro-Triguero, Evaluation of optimal sensor placement algorithms for the Structural Health Monitoring of architectural heritage. Application to the Monastery of San Jerónimo de Buenavista (Seville, Spain), Engineering Structures 202 (2020) 109843. doi:10.1016/j.engstruct.2019.109843.

[13] K. Worden, H. Sohn, C. R. Farrar, Novelty detection in a changing environment: regression and interpolation approaches, Journal of Sound and Vibration 258 (4) (2002) 741–761. doi:10.1006/jsvi.2002.5148.

[14] A. M. Yan, G. Kerschen, P. De Boe, J. C. Golinval, Structural damage diagnosis under varying environmental conditions part I: a linear analysis, Mechanical Systems and Signal Processing 19 (4) (2005) 847–864. doi:10.1016/j.ymssp.2004.12.002.

[15] A. M. Yan, G. Kerschen, P. De Boe, J. C. Golinval, Structural damage diagnosis under varying environmental conditions part II: local PCA for non-linear cases, Mechanical Systems and Signal Processing 19 (4) (2005) 865–880. doi:10.1016/j.ymssp.2004.12.003.

[16] A. Deraemaeker, E. Reynders, G. De Roeck, J. Kullaa, Vibration-based structural health monitoring using output-only measurements under changing environment, Mechanical Systems and Signal Processing 22 (1) (2008) 34 – 56. doi:10.1016/j.ymssp.2007.07.004.

[17] F. Ubertini, G. Comanducci, N. Cavalagli, A. L. Pisello, A. L. Materazzi, F. Cotana, Environmental effects on natural frequencies of the San Pietro bell tower in Perugia, Italy, and their removal for structural performance assessment, Mechanical Systems and Signal Processing 82 (2017) 307–322. doi:10.1016/j.ymssp.2016.05.025.

[18] A. Kita, N. Cavalagli, F. Ubertini, Temperature effects on static and dynamic behavior of Consoli Palace in Gubbio, Italy, Mechanical Systems and Signal Processing 120 (2019) 180–202. doi:10.1016/j.ymssp.2018.10.021.

[19] C. Gentile, M. Guidobaldi, A. Saisi, One-year dynamic monitoring of a historic tower: damage detection under changing environment, Meccanica 51 (2016) 2873 – 2889. doi:10.1007/s11012-016-0482-3.

[20] M. G. Masciotta, L. F. Ramos, P. B. Lourenço, The importance of structural monitoring as a diagnosis and control tool in the restoration process of heritage structures: a case study in Portugal, Journal of Cultural Heritage 27 (2017) 36–47. doi:10.1016/j.culher.2017.04.003.

[21] N. Cavalagli, G. Comanducci, F. Ubertini, Earthquake–induced damage detection in a monumental masonry bell-tower using long-term dynamic monitoring data, Journal of Earthquake Engineering 22 (sup1) (2018) 96–119. doi:10.1080/13632469.2017.1323048.

[22] A. Cabboi, C. Gentile, A. Saisi, From continuous vibration monitoring to FEM-based damage assessment: application on a stone-masonry tower, Construction and Building Materials 156 (2017) 252–265. doi:10.1016/j.conbuildmat.2017.08.160.

[23] M. G. Masciotta, L. F. Ramos, P. B. Lourenço, M. Vasta, Spectral algorithm for non-destructive damage localisation: Application to an ancient masonry arch model, Mechanical Systems and Signal Processing 84 (2017) 286–307. doi:10.1016/j.ymssp.2016.06.034.

[24] F. N. Catbas, T. Kijewski-Correa, Structural identification of constructed systems: Collective effort toward an integrated approach that reduces barriers to adoption, Journal of Structural Engineering 139 (10) (2013) 1648–1652. doi:10.1061/(ASCE)ST.1943-541X.0000682.

[25] W. Torres, J. L. Almazán, C. Sandoval, R. Boroschek, Operational modal analysis and FE model updating of the Metropolitan Cathedral of Santiago, Chile, Engineering Structures 143 (2017) 169–188. doi:10.1016/j.engstruct.2017.04.008.

[26] L. Vincenzi, M. Savoia, Coupling Response Surface and Differential Evolution for Parameter Identification Problems, Computer–Aided Civil and Infrastructure Engineering 30 (5) (2015) 376–393. doi:10.1111/mice.12124.

[27] E. Bassoli, L. Vincenzi, A. M. D'Altri, S. de Miranda, M. Forghieri, G. Castellazzi, Ambient vibration–based finite element model updating of an earthquake–damaged masonry tower, Structural Control and Health Monitoring 25 (5) (2018) e2150. doi:10.1002/stc.2150.

[28] I. Venanzi, A. Kita, N. Cavalagli, L. Ierimonti, F. Ubertini, Earthquake-induced damage localization in an historic masonry tower through long-term dynamic monitoring and FE model calibration, Bulletin of Earthquake Engineering 25 (2020) 1103–1122. doi:10.1007/s10518-019-00780-4.

[29] E. García-Macías, L. Ierimonti, I. Venanzi, F. Ubertini, An innovative methodology for online surrogate-based model updating of historic buildings using monitoring data, International Journal of Architectural Heritage (2019) 1–21doi:10.1080/15583058.2019.1668495.

[30] H. Sohn, K. Worden, C. R. Farrar, Novelty detection under changing environmental conditions, in: Smart Structures and Materials 2001: Smart Systems for Bridges, Structures, and Highways, Vol. 4330, International Society for Optics and Photonics, 2001, pp. 108–118.

[31] T. H. Yi, H. N. Li, H. M. Sun, Multi-stage structural damage diagnosis method based on "energy-damage" theory, Smart Structures and Systems 12 (3–4) (2013) 345–361. doi:10/d557.

[32] E. García-Macías, F. Ubertini, Seismic interferometry for earthquake-induced damage identification in historic masonry towers, Mechanical Systems and Signal Processing 132 (2019) 380–404. doi:10.1016/j.ymssp.2019.06.037.

[33] E. García-Macías, F. Ubertini, Automated operational modal analysis and ambient noise deconvolution interferometry for the full structural identification of historic towers: A case study of the Sciri Tower in Perugia, Italy, Engineering Structures 215 (2020) 110615. doi:10.1016/j.engstruct.2020.110615.

[34] E. García-Macías, F. Ubertini, MOVA/MOSS: Two integrated software solutions for comprehensive Structural Health Monitoring of structures, Mechanical Systems and Signal Processing 143 (2020) 106830. doi:10.1016/j.ymssp.2020.106830.

[35] T. H. Yi, X. J. Yao, C. X. Qu, H. N. Li, Clustering number determination for sparse component analysis during output-only modal identification, Journal of Engineering Mechanics 145 (1) (2019) 04018122. doi:10.1061/(ASCE)EM.1943-7889.0001557.

[36] Y. Xu, J. M. W. Brownjohn, D. Hester, Enhanced sparse component analysis for operational modal identification of real-life bridge structures, Mechanical Systems and Signal Processing 116 (2019) 585–605. doi:10.1016/j.ymssp.2018.07.026.

[37] M. Mitchell, An introduction to genetic algorithms, MIT press, 1998.

[38] F. E. A. Abaqus, Abaqus analysis user's manual, Dassault Systemes, Vélizy-Villacoublay, France.

[39] J. Lubliner, J. Oliver, S. Oller, E. Oñate, A plastic-damage model for concrete, International Journal of Solids and Structures 25 (3) (1989) 299–326. doi:10.1016/0020-7683(89)90050-4.

[40] J. Lee, G. L. Fenves, Plastic-damage model for cyclic loading of concrete structures, Journal of Engineering Mechanics 124 (8) (1998) 892–900. doi:10.1061/(ASCE)0733-9399(1998)124:8(892).

[41] M. Hubert, M. Debruyne, P. J. Rousseeuw, Minimum covariance determinant and extensions, Wiley Interdisciplinary Reviews: Computational Statistics 10 (3) (2018) e1421. doi:10.1002/wics.1421.

[42] C. Gentile, A. Ruccolo, A. Saisi, Continuous dynamic monitoring to enhance the knowledge of a historic bell-tower, International Journal of Architectural Heritage 13 (7) (2019) 992–1004. doi:10.1080/15583058.2019.1605552.